

This is the accepted manuscript made available via CHORUS. The article has been published as:

## Beyond the pair approximation: Modeling colonization population dynamics

Ignacio A. Rodriguez-Brenes, Dominik Wodarz, and Natalia L. Komarova

Phys. Rev. E **101**, 032404 — Published 6 March 2020

DOI: [10.1103/PhysRevE.101.032404](https://doi.org/10.1103/PhysRevE.101.032404)

# Beyond the pair approximation: modeling colonization population dynamics

Ignacio A. Rodriguez-Brenes<sup>1,\*</sup>, Dominik Wodarz<sup>2</sup>,  
Natalia L. Komarova<sup>1,\*</sup>

<sup>1</sup> Department of Mathematics;

<sup>2</sup> Department of Ecology and Evolutionary Biology, University of California Irvine, Irvine, CA 92697

\* Corresponding authors: ignacio.rodriguez-brenes@uci.edu, komarova@uci.edu

**Abstract.** The process of range expansion (colonization) is one of the basic types of biological dynamics, whereby a species grows and spreads outwards, occupying new territories. Spatial modeling of this process is naturally implemented as a stochastic cellular automaton, with individuals occupying nodes on a rectangular grid, births and deaths occurring probabilistically, and individuals only reproducing unto unoccupied neighboring spots. In this paper we derive several approximations that allow prediction of the expected range expansion dynamics, based on the reproduction and death rates. We derive several approximations, where the cellular automaton is described by a system of ODEs that preserves correlations amongst neighboring spots (up to a distance). This methodology allows us to develop accurate approximations of the population size and the expected spatial shape, at a fraction of the computational time required to simulate the original stochastic system. In addition, we provide simple formulas for the steady-state population densities for von Neumann and Moore neighborhoods. Finally, we derive concise approximations for the speed of range expansion in terms of the reproduction and death rates, for both types of neighborhoods. The methodology is generalizable to more complex scenarios, such as different interaction ranges and multiple-species systems.

## 1 Introduction

Range expansion, or colonization, is the process in biology by which a species spreads to new areas. Examples include: The growth of microorganisms to form 2D formations called biofilms [1]; the spread of solid tumors in 2D and 3D [2] (including the formation of spheroids in vitro [3] and the growth of cell cultures in 2D and 3D [4]); the growth of bacterial and viral/bacteriophage plaques [5–7]; and even the growth of human settlements [8,9]. It is well known that spatial population expansion is very different from the exponential growth experienced by well mixed systems, and yet mathematical tools appropriate for the description of range expansion are not fully developed.

Mathematical models of colonization processes vary in methodology and sophistication. One popular approach are stochastic cellular automata. See [10], for example, for a review of their use in tumor modeling, [11] for a review of applications to urban development, and also [2,12–14]. In these models, individuals are located on a fixed grid, and stochastic rules govern births and deaths. This versatile approach has proven to be a valuable tool for computational studies of range expansion and various related phenomena. It is conceptually simple, but also a significant improvement compared to ordinary differential equations, because it is both stochastic and spatial. This approach, however, can be computationally very costly, making it difficult to extract from

simulations statistics on the time-evolution of a system, especially when population sizes are large. Furthermore, exact analytical descriptions of these models, such as those obtain via the Kolmogorov or Master Equations [15] are usually intractable.

Some of the most common simplified descriptions of cellular automata (also known as agent-based models) are derived from mean-field behavior. These include deterministic reaction-diffusion equations, such as Fisher’s equation [16]. Mean-field approximations, however, neglect the important effects of spatial correlations. As a consequence most of these models provide inaccurate descriptions of the average trajectories of stochastic agent-based models. The next level of complexity is the so called pair approximation, see e.g. [17–24]. This methodology has been used in an attempt to capture certain aspects of spatial dynamics by more tractable means. It can be successful at predicting equilibrium properties of a system, but in general does not provide good time-series agreement with the corresponding stochastic process [25].

In this paper we develop deterministic spatially explicit approximations for the expected trajectories of a two-dimensional stochastic birth-death process implemented as an agent-based model. The approximations provide an accurate description of the expected time-evolution of the system. In particular, we focus on modeling population growth expanding radially from an origin  $o$ , and compare our results with the traditional pair approximation and mean-field models.

We also derive simple approximate formulas for the steady-state population densities based on the death rate,  $D$ , and reproduction rate,  $L$ , of individuals. While in a well-mixed non-spatial setting (mass action), the equilibrium density,  $\rho_{ma}$ , is given by

$$\rho_{ma} = 1 - \frac{D}{L}, \quad (1)$$

in spatially restricted populations this quantity is lower. We find that in the case of the von Neumann neighborhood (4 neighbors), the density can be approximated by

$$\rho_{vN} = \left(3 - 4\frac{D}{L}\right) \left(3 - \frac{D}{L}\right)^{-1} \quad (2)$$

(where the subscript  $vN$  stands for “von Neumann”), in the case of the hexagonal (honeycomb) lattice, where each node has six nearest neighbors, we have

$$\rho_H = \left(5 - 6\frac{D}{L}\right) \left(5 - \frac{D}{L}\right)^{-1} \quad (3)$$

(where  $H$  stands for “hexagonal”), and in the case of the Moore neighborhood (8 neighbors), it is approximately given by

$$\rho_M = \left(7 - 8\frac{D}{L}\right) \left(7 - \frac{D}{L}\right)^{-1} \quad (4)$$

(where the subscript  $M$  stands for “Moore”). The general formula that describes these spatial approximations is

$$\rho(n) = \left(n - 1 - n\frac{D}{L}\right) \left(n - 1 - \frac{D}{L}\right)^{-1}, \quad (5)$$

where  $n$  is the number of neighbors in the grid’s geometry. This formula holds also for a 3D square lattice, both for the Moore and von Neumann neighborhoods. Note that in (5) the limit as  $n \rightarrow \infty$  recovers the equilibrium density for mass action (1), where the number of neighbors is infinite.

Finally, we develop concise approximations for the expected speed of range expansion in an infinite grid. We end by discussing extensions of the theory –including three-dimensional growth, different grid geometries, and multiple species– and several important evolutionary and biological applications.

## 2 Spatially explicit decoupling approximations

### 2.1 Preliminaries

We begin by considering a birth-death process on a 2D rectangular lattice. Let the value of the site with coordinates  $(i, j)$  at time  $t$  be  $x_{ij}(t) = 0$  if the site is empty, and  $x_{ij}(t) = 1$  if it is occupied. We consider the  $\ell_1$  distance in the lattice, i.e.,  $\text{dist}(x_{ij}, x_{lk}) = |i - l| + |j - k|$ . Defining nearest neighbors as sites that lie one unit of distance apart from each other, we introduce a notation for the four nearest neighbors of a site  $x_{ij}$ : We write  $x_{ij}^{(1)} = x_{i-1,j}$ ,  $x_{ij}^{(2)} = x_{i+1,j}$ ,  $x_{ij}^{(3)} = x_{i,j-1}$ ,  $x_{ij}^{(4)} = x_{i,j+1}$ . Note that a site and its four nearest neighbors make up a von Neumann neighborhood of radius one. Finally, we assume that individuals reproduce stochastically onto each unoccupied nearest neighboring site with a rate  $L/4$ , and die at a rate  $D$ .

Figure 1B plots the expected number of individuals as function of time. We implement the process as a stochastic agent-based model on a finite grid with periodic boundary conditions using the next reaction method [26] (thick solid line). Here, starting from an initial small cluster of cells at the grid's center, the expected number of individuals first increases and then plateaus as the population colonizes the entire grid. Figure 1A depicts, as a heatmap, the spatial configuration of the expected number of individuals at a time before the entire grid is colonized.

If we use angular brackets to denote the expected value, we find that the stochastic process results in the following equation:

$$\frac{d\langle x_{ij} \rangle}{dt} = \left\langle \frac{L}{4}(1 - x_{ij}) \sum_{s=1}^4 x_{ij}^{(s)} - D x_{ij} \right\rangle \quad (6)$$

If we neglect correlations in (6) and assume that for any pair of sites  $a$  and  $b$ ,  $\langle ab \rangle = \langle a \rangle \langle b \rangle$ , we arrive at the spatial mean-field model:

$$\frac{d\langle x_{ij} \rangle}{dt} = \frac{L}{4}(1 - \langle x_{ij} \rangle) \sum_{s=1}^4 \langle x_{ij}^{(s)} \rangle - D \langle x_{ij} \rangle \quad (7)$$

Figure 1B demonstrates that the mean-field model is not a very accurate representation of the average behavior of the stochastic process (compare dotted and thick solid lines).

To improve upon the mean-field approximation we note that (6) introduces terms of the form  $\langle x_{ij} x_{i+1,j} \rangle$  and  $\langle x_{ij} x_{i,j+1} \rangle$ , which require new equations to describe their rate of change. These are:

$$\frac{d\langle x_{ij} x_{i+1,j} \rangle}{dt} = \left\langle \frac{L}{4}(1 - x_{ij}) \sum_{s=1}^4 x_{ij}^{(s)} x_{i+1,j} + \frac{L}{4}(1 - x_{i+1,j}) \sum_{s=1}^4 x_{i+1,j}^{(s)} x_{ij} - 2D x_{ij} x_{i+1,j} \right\rangle \quad (8)$$

$$\frac{d\langle x_{ij} x_{i,j+1} \rangle}{dt} = \left\langle \frac{L}{4}(1 - x_{ij}) \sum_{s=1}^4 x_{ij}^{(s)} x_{i,j+1} + \frac{L}{4}(1 - x_{i,j+1}) \sum_{s=1}^4 x_{i,j+1}^{(s)} x_{ij} - 2D x_{ij} x_{i,j+1} \right\rangle \quad (9)$$

Equations (8) and (9) introduce terms of the form  $\langle bc \rangle$  and  $\langle abc \rangle$ , where  $a, b$ , and  $c$  are sites in the grid that satisfy  $\text{dist}(a, b) = \text{dist}(a, c) = 1$ , and  $\text{dist}(b, c) = 2$ . In principle, these new terms require additional equations that involve higher order moments. At some point however, we need to cut off the process of adding equations and instead use approximations to obtain a closed system.

## 2.2 Spatially explicit decoupling approximations and the pair approximation

Before proceeding, we need to establish notation and some fundamental relations. First, note that for any triad of sites  $\{a, b, c\}$ , the following relation always holds:  $\langle bc \rangle - \langle abc \rangle = P(b = 1, a = 0, c = 1)$ . Let  $P_{ijk}$  be defined by

$$\begin{aligned} P_{ij1} &= P(x_{i-1,j} = 1, x_{ij} = 0, x_{i+1,j} = 1), \\ P_{ij2} &= P(x_{i,j-1} = 1, x_{ij} = 0, x_{i,j+1} = 1), \\ P_{ij3} &= P(x_{i-1,j} = 1, x_{ij} = 0, x_{i,j-1} = 1), \\ P_{ij4} &= P(x_{i,j-1} = 1, x_{ij} = 0, x_{i+1,j} = 1), \\ P_{ij5} &= P(x_{i+1,j} = 1, x_{ij} = 0, x_{i,j+1} = 1), \\ P_{ij6} &= P(x_{i-1,j} = 1, x_{ij} = 0, x_{i,j+1} = 1). \end{aligned} \tag{10}$$

If we call  $U_{ij} = \langle x_{ij} \rangle$ ,  $Y_{ij1} = \langle x_{ij} x_{i+1,j} \rangle$  and  $Y_{ij2} = \langle x_{ij} x_{i,j+1} \rangle$ , then the system (6)-(9) can be rewritten succinctly as:

$$\begin{aligned} \dot{U}_{ij} &= \frac{L}{4} (U_{i-1,j} - Y_{i-1,j,1} + U_{i+1,j} - Y_{ij1} + U_{i,j-1} - Y_{i,j-1,2} + U_{i,j+1} - Y_{ij2}) - DU_{ij}, \\ \dot{Y}_{ij1} &= \frac{L}{4} (U_{ij} + U_{i+1,j} - 2Y_{ij1} + P_{ij1} + P_{ij4} + P_{ij5} + P_{i+1,j,1} + P_{i+1,j,3} + P_{i+1,j,6}) - 2DY_{ij1}, \\ \dot{Y}_{ij2} &= \frac{L}{4} (U_{ij} + U_{i,j+1} - 2Y_{ij2} + P_{ij2} + P_{ij5} + P_{ij6} + P_{i,j+1,2} + P_{i,j+1,3} + P_{i,j+1,4}) - 2DY_{ij2}. \end{aligned} \tag{11}$$

The presence of the  $P_{ijk}$  in (11) means that this system is not closed. To close it, let us consider the following relations, where, as before  $\text{dist}(a, b) = \text{dist}(a, c) = 1$ , and  $\text{dist}(b, c) = 2$ :

$$\begin{aligned} P(b = 1, a = 0, c = 1) &= P(b = 1|a = 0, c = 1)P(a = 0, c = 1) \\ &\approx P(b = 1|a = 0)P(a = 0, c = 1) \\ &= (\langle b \rangle - \langle ab \rangle) / (1 - \langle a \rangle)(\langle c \rangle - \langle ac \rangle). \end{aligned} \tag{12}$$

Intuitively, the approximation  $P(b|a = 0, c = 1) \approx P(b = 1|a = 0)$  assumes that the probability that a site is equal to one is only weakly dependent on the probability that another site two units of distance apart is also equal to one. Now, let  $\delta_{ij} = 1/(1 - U_{ij})$  if  $U_{ij} < 1$  and  $\delta_{ij} = 0$  otherwise. If we define the  $B_{ijk}$  by

$$\begin{aligned} B_{ij1} &= (U_{i+1,j} - Y_{ij1})(U_{i-1,j} - Y_{i-1,j,1}), \\ B_{ij2} &= (U_{i,j-1} - Y_{i,j-1,2})(U_{i,j+1} - Y_{ij2}), \\ B_{ij3} &= (U_{i,j-1} - Y_{i,j-1,2})(U_{i-1,j} - Y_{i-1,j,1}), \\ B_{ij4} &= (U_{i,j-1} - Y_{i,j-1,2})(U_{i+1,j} - Y_{ij1}), \\ B_{ij5} &= (U_{i+1,j} - Y_{ij1})(U_{i,j+1} - Y_{ij2}), \\ B_{ij6} &= (U_{i-1,j} - Y_{i-1,j,1})(U_{i,j+1} - Y_{ij2}), \end{aligned} \tag{13}$$

then using (12), we arrive at the approximations  $P_{ijk} \approx \delta_{ij} B_{ijk}$ . We call these approximations *spatially explicit decoupling approximation*, or SEDA. Finally, substituting the  $P_{ijk}$  in (11) yields

the following closed-form approximation for the system:

$$\begin{aligned}
\dot{U}_{ij} &= \frac{L}{4} [U_{i-1,j} - Y_{i-1,j,1} + U_{i+1,j} - Y_{ij1} + U_{i,j-1} - Y_{i,j-1,2} + U_{i,j+1} - Y_{ij2}] - DU_{ij}, \\
\dot{Y}_{ij1} &= \frac{L}{4} [U_{ij} + U_{i+1,j} - 2Y_{ij1} + \delta_{ij}(B_{ij1} + B_{ij4} + B_{ij5}) + \delta_{i+1,j}(B_{i+1,j,1} + B_{i+1,j,3} + B_{i+1,j,6})] \\
&\quad - 2DY_{ij1}, \\
\dot{Y}_{ij2} &= \frac{L}{4} [U_{ij} + U_{i,j+1} - 2Y_{ij2} + \delta_{ij}(B_{ij2} + B_{ij5} + B_{ij6}) + \delta_{i,j+1}(B_{i,j+1,2} + B_{i,j+1,3} + B_{i,j+1,4})] \\
&\quad - 2DY_{ij2}.
\end{aligned} \tag{14}$$

System (14) preserves information of neighbors up to one unit of distance apart in the  $\ell_1$  metric, for this reason we refer to this model as 1<sup>st</sup> order SEDA. Similarly, using the same type of approximation, we can construct a model that preserves correlations of neighbors that lie up  $n$  units of distance apart from each other; we refer to this model as  $n^{\text{th}}$  order SEDA. Note that throughout this paper, when we make reference to a SEDA approximation without specifying the order, we are referring to a 1<sup>st</sup> order approximation. In Appendix A and B we give general rules for higher order SEDA and present the formulae for 2<sup>nd</sup> order, which requires 24 differential equations per point (instead of the just three required in (14)).

We can recover the traditional so called *pair approximations* (PA) from the 1<sup>st</sup> order SEDA equations (14). To do so, let us first define  $U$  as the total number of individuals,  $N$  as the number of sites in the grid, and  $Y$  as the average correlation between any two nearest neighbors times  $N$ . To derive the PA equations from (14) we need to: (i) set the  $\delta_{ij} = 1$ , which in SEDA prevent singularities at individual sites; (ii) assume spatial homogeneity, that is,  $U = NU_{ij}$  and  $Y = NY_{ij1}$  for any  $(i, j)$ ; and (iii) set  $Y_{ij2} = Y_{ij1}$ . The PA equations for the birth-death process are:

$$\begin{aligned}
\dot{U} &= L(U - Y) - DU \\
\dot{Y} &= \frac{L}{2}(U - Y) + \frac{3L}{2}(U - Y)^2/(N - U) - 2DY
\end{aligned} \tag{15}$$

We remark on two key differences between PA and SEDA: 1) PA models are non-spatial. They track only the total number of individuals, but not the spatial location of each individual. 2) PA models only consider correlations of pairs, while depending on the order, SEDA models can preserve correlations for larger groups of neighbors (e.g., up to quintuplets in 2<sup>nd</sup> order equations).

Figure 1B plots the expected number of individuals as a function of time, calculated from stochastic simulations, the mean-field model, 1<sup>st</sup> and 2<sup>nd</sup> order SEDA, and PA. It is clear from this figure that 1<sup>st</sup> order SEDA is closer to the results from the stochastic process than the PA or mean-field models. We also see that 2<sup>nd</sup> order improves on the 1<sup>st</sup> order approximation, but the agreement with the stochastic results is still far from optimal. In section 3, we will build on 1<sup>st</sup> order SEDA to find more accurate deterministic representations of the expected behavior of the stochastic process.

### 3 Radial decoupling, trigonometric approximations, and time-scaling SEDA

In this section we provide methods to improve the SEDA description of range expansion, to reach nearly-perfect approximations in a wide range of parameters. We first develop a new approximation, which we call radial decoupling approximation. We then combine this radial approximation with SEDA, to find a method that produces much better agreement with the stochastic process than

$\mathcal{P}_{abc}$	$\theta_{abc}$	$\theta_{oa} \in [\theta_{abc}, \theta_{abc} + \pi)$	$\theta_{oa} \notin [\theta_{abc}, \theta_{abc} + \pi)$	$\alpha_{ijk}$
$P_{ij1}$	$\pi$	$A_{ij1} = U_{i+1,j} - Y_{ij1}$	$A_{ij1} = U_{i-1,j} - Y_{i-1,j,1}$	$c_{\cos} \cos(2\theta_{ij}) + m_{\cos}$
$P_{ij2}$	$\pi/2$	$A_{ij2} = U_{i,j-1} - Y_{i,j-1,2}$	$A_{ij2} = U_{i,j+1} - Y_{ij2}$	$-c_{\cos} \cos(2\theta_{ij}) + m_{\cos}$
$P_{ij3}$	$3\pi/4$	$A_{ij3} = U_{i,j-1} - Y_{i,j-1,2}$	$A_{ij3} = U_{i-1,j} - Y_{i-1,j,1}$	$-c_{\sin} \sin(2\theta_{ij}) + m_{\sin}$
$P_{ij4}$	$\pi/4$	$A_{ij4} = U_{i,j-1} - Y_{i,j-1,2}$	$A_{ij4} = U_{i+1,j} - Y_{ij1}$	$c_{\sin} \sin(2\theta_{ij}) + m_{\sin}$
$P_{ij5}$	$3\pi/4$	$A_{ij5} = U_{i+1,j} - Y_{ij1}$	$A_{ij5} = U_{i,j+1} - Y_{ij2}$	$-c_{\sin} \sin(2\theta_{ij}) + m_{\sin}$
$P_{ij6}$	$\pi/4$	$A_{ij6} = U_{i-1,j} - Y_{i-1,j,1}$	$A_{ij6} = U_{i,j+1} - Y_{ij2}$	$c_{\sin} \sin(2\theta_{ij}) + m_{\sin}$

Table 1: Columns 1 to 4: Radial decoupling approximation,  $A_{ijk}$ , of  $P_{ijk}$ , based on the angle  $\theta_{oa}$  from  $v_o$  to  $\vec{o}\vec{a}$  (see text). Columns 1 and 5: Trigonometric coefficients  $\alpha_{ijk}$  for each  $P_{ijk}$ . Note that  $\theta_{oa} = \theta_{ij}$  (same angle different notation).

pure SEDA alone. We call this combined method trigonometric decoupling approximation. Finally, we introduce an alternative, time-scaling approach that also improves SEDA results.

### 3.1 Radial decoupling approximations

In section 2.2, we used approximation (12) for quantity  $\mathcal{P}_{abc} = P(b=1, a=0, c=1)$ , where  $a, b$  and  $c$  are sites in the grid, that satisfy  $\text{dist}(a, b) = \text{dist}(a, c) = 1$ , and  $\text{dist}(b, c) = 2$  (note that sub-indexes in  $\mathcal{P}_{abc}$  are sites and not coordinates). Here, we develop a different approximation for this quantity. We focus on modeling 2D growth expanding radially from an origin  $o$ , with coordinates  $(i_o, j_o)$ .

We begin by noting the following relations:

$$\mathcal{P}_{abc} = P(b=1|a=0, c=1)P(a=0, c=1) \quad (16)$$

$$= P(c=1|a=0, b=1)P(a=0, b=1). \quad (17)$$

Numerical simulations show that, as time proceeds, soon after  $\mathcal{P}_{abc}$  increases from its initial zero value,  $P(b=1|a=0, c=1)$  or  $P(c=1|a=0, b=1)$  remains relatively stable. Then, given that  $P(a=0, b=1) = \langle b \rangle - \langle ab \rangle$  and  $P(a=0, c=1) = \langle c \rangle - \langle ac \rangle$ , the previous observation and eqs. (16–17) suggest the approximations:  $\mathcal{P}_{abc} \approx \eta(\langle c \rangle - \langle ac \rangle)$  or  $\mathcal{P}_{abc} \approx \eta(\langle b \rangle - \langle ab \rangle)$ , where  $\eta$  is the stationary value for  $P(c=1|a=0, b=1)$  and  $P(b=1|a=0, c=1)$  (i.e. for time  $t$  large). We call these approximations *radial decoupling approximations*, or RDA.

We now describe a procedure to decide which of the two approximations ( $\mathcal{P}_{abc} \approx \eta(\langle c \rangle - \langle ac \rangle)$  or  $\mathcal{P}_{abc} \approx \eta(\langle b \rangle - \langle ab \rangle)$ ) to use, based on the geometry of the triad  $\{a, b, c\}$  and the the location of  $a$  relative to the origin  $o$ . First, we can think of  $a$  (with coordinates  $(i_a, j_a)$ ) as the center of the triad. There is a unique line  $\ell$  that goes through  $a$  and is perpendicular to the vector  $\vec{bc}$ , see Figure 2. This line divides the plane into two half-planes:  $H_b$ , which contains the site  $b$ , and  $H_c$ , which contains the site  $c$ . Let  $v_a$  be the vector that goes from  $a$  to the site with coordinates  $(i_a, j_a + 1)$ . We can then define  $\theta_{abc}$  as the angle between  $v_a$  and  $\ell$  measured in a counterclockwise direction. Given the geometry of the grid,  $\theta_{abc}$  will take on one the values  $\pi/4$ ,  $\pi/2$ ,  $3\pi/4$ , or  $\pi$  (Figure 2). If we measure angles based on the interval  $[0, 2\pi)$ , one of the half-planes discussed will be made up of those sites  $e$ , where the angle from  $v_a$  to  $\vec{a}\vec{e}$  (measured counterclockwise) lies between  $\theta_{abc}$  and  $\theta_{abc} + \pi$ . To simplify the notation let us assume that this half-plane is  $H_b$ . Now, let  $v_o$  be the vector from  $o$  to the site with coordinates  $(i_o, j_o + 1)$ . If the angle  $\theta_{oa}$  from  $v_o$  to  $\vec{o}\vec{a}$  is such that

$\theta_{abc} \leq \theta_{oa} < \theta_{abc} + \pi$ , use the approximation  $\mathcal{P}_{abc} \approx \eta(\langle b \rangle - \langle ab \rangle)$ ; otherwise, use  $\mathcal{P}_{abc} \approx \eta(\langle c \rangle - \langle ac \rangle)$ . To further simplify the notation, in the future we will also refer to  $\theta_{oa}$  as  $\theta_{ij}$ .

The procedure/algorithm described in the previous paragraph is informed by simulation results. The critical time to model  $\mathcal{P}_{abc}$  is during the transitional time period where this quantity changes from a near zero state to its long term stationary value. During this transitional period, the triad  $\{a, b, c\}$  is located near the edge of the radially expanding population. Simulation results indicate that the best RDA is the one that explicitly tracks information from the site (either  $b$  or  $c$ ) that is most likely to lie outside the radially expanding population during this transitional time. Intuitively this makes sense. Because the expected value of a site that lies outside the expanding population is more likely to change during this time, than the expected value of a site that lies inside the population mass, where it is more likely to be near its long term steady-state. The algorithm described in the previous paragraph selects the best RDA according to this criteria.

Table 1 specifies how to choose the RDA for the  $P_{ijk}$  in (10). Following the definitions of the  $A_{ijk}$  in this table, the approximations can be written succinctly as  $P_{ijk} \approx \eta A_{ijk}$ . A closed-form approximation for system (11) then follows by substituting the  $P_{ijk}$  by  $\eta A_{ijk}$  in (11). We can determine  $\eta$  by considering the equations of the new system at equilibrium. We do so by setting the equations equal zero, dropping the subscripts, and solving for  $\eta$ . We find  $\eta = 1 - \frac{4D}{3L}$ , which suggests a valid approximation for  $D/L < 0.75$ . This equilibrium analysis, however, also reveals that, unlike the stochastic process, a system based only on RDA does not have a unique non-trivial steady state. Instead, we discover that combining RDA with SEDA restores a unique equilibrium to the system and provides very accurate results. We discuss this combined approach next.

### 3.2 Trigonometric approximation

Before we proceed we can introduce a small correction by modifying the SEDA model so that its steady-state density more closely matches that of the corresponding stochastic process. The procedure consists of substituting the approximation  $P_{ijk} \approx \delta_{ij} B_{ijk}$  by  $P_{ijk} \approx \min(\epsilon \delta_{ij} B_{ijk}, 1)$ , where  $\epsilon \geq 1$ . Using the notation of section 3.1 this implies that on average  $P(b = 1|a = 0, c = 1) \geq P(b = 1|a = 0)$ . This intuitively makes sense, because being at most two units of distance apart from each other, the values of  $b$  and  $c$  are correlated. To determine  $\epsilon$ , we can substitute the steady-state densities of the stochastic process,  $U_s$  and  $Y_s$ , with the modified approximations for  $P_{ijk}$  into (14), set these equations equal to zero, and solve for  $\epsilon$ ; this yields:

$$\epsilon = \left( \frac{L}{D} - \frac{4}{3} \right) (1 - U_s) U_s^{-1}. \quad (18)$$

Note that  $U_s$  and  $Y_s$  are independent of grid size. Hence using (18), for any ratio  $D/L$  we can compute the value of  $\epsilon$  from simulations in a small grid. After calculating several of these values, we can find a formula for  $\epsilon$  using polynomial regression (See Figure A2 in the Appendix):

$$\epsilon = 1.85(D/L)^3 - 0.46(D/L)^2 + 0.045(D/L) + 1 \quad (19)$$

We now introduce a method to combine SEDA and RDA for the probabilities  $P_{ijk}$ . One approach is to weight the two types of approximations and add them up. More precisely, let  $\alpha_{ijk} \in [0, 1]$ , we consider approximations of the form:

$$P_{ijk} \approx C_{ijk} = \alpha_{ijk} \underbrace{\min(\epsilon \delta_{ij} B_{ijk}, 1)}_{\text{SEDA}} + (1 - \alpha_{ijk}) \underbrace{\left(1 - \frac{4D}{3L}\right) A_{ijk}}_{\text{RDA}} \quad (20)$$

Next, we need to determine appropriate values for the weights  $\alpha_{ijk}$ . We begin by exploring the problem numerically, with a focus on modeling 2D growth expanding radially from an origin



o. For a given grid size and set of parameters,  $D$  and  $L$ , we can run multiple simulations past the point where the system reaches its stationary distribution. From these simulations we can compute the statistics (known as sample statistics)  $\overline{P}_{ijk}(t)$ ,  $\overline{\delta_{ij}B}_{ijk}(t)$ , and  $\overline{A}_{ijk}(t)$ . We can then define  $\hat{\alpha}_{ijk}$  as the parameter  $\alpha_{ijk} \in [0, 1]$  that minimizes  $\|\overline{P}_{ijk}(t) - (\alpha_{ijk} \min(\epsilon \overline{\delta_{ij}B}_{ijk}(t), 1) + (1 - \alpha_{ijk})(1 - \frac{4D}{3L})\overline{A}_{ijk}(t))\|_{\ell_1}$ . Intuitively,  $\hat{\alpha}_{ijk}$  provides the best approximation possible for  $P_{ijk}$  that uses equation (20). Figure A4 shows that these “best fit” combined approximations (i.e., using the  $\hat{\alpha}_{ijk}$ ), provide a significant improvement over the pure SEDA approximations. Figure 3A plots the coefficients  $\hat{\alpha}_{ij1}$  vs. the angles  $\theta_{ij}$  (dots). The plot shows that the coefficients are approximately periodic with the angles, which suggests that we could use a trigonometric formula for the  $\alpha_{ij1}$ . Indeed, the black curve in this figure is the function  $c_{\cos} \cos(2\theta) + m_{\cos}$ . To determine the parameters  $c_{\cos}$  and  $m_{\cos}$ , we average the  $\hat{\alpha}_{ij1}$  that have the same  $\theta_{ij}$ ; for a given angle  $\theta$  let this average be  $\alpha_1(\theta)$ . We then use a basic optimization procedure to find the parameters,  $c_{\cos}$  and  $m_{\cos}$  that minimize  $\|\alpha_1(\theta) - (c_{\cos} \cos(2\theta) + m_{\cos})\|_{\ell_1}$  (Figure 3B). Similarly, Figure 3C plots the averages,  $\alpha_4(\theta)$  and  $\alpha_6(\theta)$ , computed from the coefficients  $\hat{\alpha}_{ij4}$  and  $\hat{\alpha}_{ij6}$ . In this case, the trigonometric formula for the  $\alpha_{ij4}$  and  $\alpha_{ij6}$  has the form  $c_{\sin} \sin(2\theta_{ij}) + m_{\sin}$  (thick line). Note here that the fitting of  $\alpha_4$  and  $\alpha_6$  would not benefit from a phase shift, because the error data do not exhibit the same symmetry as the sine function does. Instead, the sine approximation mostly lies between  $\alpha_4$  and  $\alpha_6$ . However, since  $\alpha_4$  and  $\alpha_6$  appear in tandem in the ODEs, the net effect will produce an overall very good fit. We find then that the formulae for the six coefficients  $\alpha_{ijk}$  ( $k = 1, \dots, 6$ ), can be expressed in terms of four parameters,  $c_{\cos}, m_{\cos}, c_{\sin}$  and  $m_{\sin}$ , as described by Table 1. We call the approximations that use the  $\alpha_{ijk}$  in this table, *trigonometric decoupling approximation*, or TDA. Compared to SEDA, TDA produce significantly smaller errors approximating the probabilities  $P_{ijk}$  (Figure A5).

Finally, Figure 4 plots the expected number of individuals as a function of time. In each panel stochastic simulations are compared to results from the mean-field model, SEDA, and TDA, for different death rates and grid sizes. In this figure the trigonometric approximation improves with grid size. This behavior is caused by the periodic boundary conditions used in the simulations, which are not specifically accounted for in the formulae for the  $\alpha_{ijk}$ . Hence, as the grid size increases and the contribution of the boundary effects to the overall population diminishes, the trigonometric approximation improves. We see this in Figure 4, once grid size is sufficiently large, the agreement between the TDA model and simulation results is excellent.

We calculated the coefficients  $c_{\cos}, m_{\cos}, c_{\sin}, m_{\sin}$  for different values of  $D/L$  and then fitted the data with polynomial functions (Figure A3) using least-squares in grids of size  $45 \times 45$ ; these polynomial regressions yield the equations in (21), and their validity was verified for grids roughly 8, 500, and 5000 times larger (Figures 4 and 6). Together equations (13), (20–22), and Table 1 provide a full and explicit formula for the TDA model. This approximation is very successful for  $D/L \leq 0.4$ , which roughly corresponds to steady-state densities  $\geq 50\%$ .

$$\begin{aligned} c_{\cos} &= 0.39(D/L)^2 - 0.46(D/L) + 0.24, \\ c_{\sin} &= -2.4(D/L)^3 + 2.1(D/L)^2 - 0.72(D/L) + 0.22, \\ m_{\cos} &= -9.7(D/L)^3 + 7.5(D/L)^2 - 2(D/L) + 0.59, \\ m_{\sin} &= -8.6(D/L)^3 + 5.3(D/L)^2 - 1.4(D/L) + 0.46 \end{aligned} \tag{21}$$

$$\begin{aligned} \dot{U}_{ij} &= \frac{L}{4} (U_{i-1,j} - Y_{i-1,j,1} + U_{i+1,j} - Y_{ij1} + U_{i,j-1} - Y_{i,j-1,2} + U_{i,j+1} - Y_{ij2}) - DU_{ij}, \\ \dot{Y}_{ij1} &= \frac{L}{4} (U_{ij} + U_{i+1,j} - 2Y_{ij1} + C_{ij1} + C_{ij4} + C_{ij5} + C_{i+1,j,1} + C_{i+1,j,3} + C_{i+1,j,6}) - 2DY_{ij1}, \\ \dot{Y}_{ij2} &= \frac{L}{4} (U_{ij} + U_{i,j+1} - 2Y_{ij2} + C_{ij2} + C_{ij5} + C_{ij6} + C_{i,j+1,2} + C_{i,j+1,3} + C_{i,j+1,4}) - 2DY_{ij2} \end{aligned} \tag{22}$$

### 3.3 Time-scaling SEDA

For each grid site  $(i, j)$  there is a transient time period where the values of the approximations  $\delta_{ijk}B_{ijk} < P_{ijk}$  (compare blue and yellow lines in Figure A4 in the Appendix). During this time period, the derivative of  $U_{ij}$  calculated using SEDA is larger than the same derivative according to the stochastic process. As a consequence, before reaching the steady state, system (14) overestimates the total number of individuals as a function of time (Figures 1 and 4). Heuristically, these observations suggest that by scaling time by a parameter  $\alpha_{D/L} \leq 1$  in (14), we can improve the quality of the approximation. More precisely if  $S$  is the total number of individuals and (14) yields the functional relation  $S = F(t)$ , then we can improve the approximation by setting  $S = F(\alpha_{D/L}t)$ , where the value of  $\alpha_{D/L}$  is determined through least-squares fitting in a small grid (Figure 5). We can then find through polynomial regression a formula for  $\alpha_{D/L}$  valid for  $D/L \leq 0.4$ :

$$\alpha_{D/L} = (1.72(D/L)^2 + 0.0795(D/L) + 1.3)^{-1} \quad (23)$$

We tested equations (21) for the trigonometric parameters and (23) for the  $\alpha_{D/L}$  in much larger grids (Figure 6). As initial conditions we used random plaques grown stochastically from an initial set of 13 occupied sites at the center of the grid (left image of each panel). Here the sizes of the initial plaques are large enough so that with them as initial conditions the trajectories of the total number of individuals as a function time behave almost deterministically; and hence, a single stochastic run is sufficient to track the time evolution of the expected number of individuals. We find that (21) and (23) produce very good approximations, in much larger grids with random plaques as initial conditions.

Next, we discuss the numerical solution of the approximate systems. These systems of course can be solved using higher order implicit methods, such as Runge-Kutta, which is the standard method, and unless stated otherwise, is behind the figures in the paper. However, we are interested in evaluating the performance and accuracy of forward Euler, as this method is the simplest to implement and fastest to compute. We found that in forward Euler a step size of  $dt = 0.025L$  provides good results for  $0.25 \leq D/L \leq 0.4$  and a step size of  $dt = 0.0125L$  is sufficient for all  $D/L \leq 0.4$ . The approximate systems yield very large improvements in computational performance compared to stochastic simulations for large grids. For example, for the simulations in Figure 6B, with a grid size of  $\approx 10^7$  sites, and a death-to-birth ratio  $D/L = 0.25$ , before reaching saturation the trigonometric approximation was more than 100 times faster than a single stochastic run.

Finally, we note that applying the rescaling procedures described in this section to PA or the spatial mean-field model does not produce satisfactorily results (section F in the Appendix). Indeed, besides PA being non-spatial, the curve shapes of a rescaled PA and the stochastic results are substantially different (Figure A8). Also, rescaling the spatial mean-field model easily results in high relative errors and very inaccurate approximations to the stochastic process at early times  $t$  (Figure A9).

## 4 Steady-state density

Here we focus on the steady-state behavior of the spatial birth death process, and derive several approximations for the steady-state density. We note that up to this point we have only dealt with von Neumann neighborhoods. In this and the next section we also consider Moore neighborhoods in relation to both steady-state and range expansion results. For a derivation of the steady-state formulas in 3D see Appendix G.

## 4.1 Steady-state density for the von Neumann neighborhood

As seen from the long term dynamics in Figure 1B, in a finite grid, the expected population size eventually reaches a steady state. We can calculate the steady-state density predicted by the mean-field approximation by dropping the subscripts in (7) and setting the right hand side of the equation to zero. Solving this equation, we find that the steady-state density in the mean-field model is equal to that of mass action (formula (1)). Here mass action refers to the well-mixed non-spatial version of the birth death process, described by equation  $\dot{X} = LX(1 - X/K) - DX$ , where  $X$  is the total number of individuals,  $K$  the system's carrying capacity, and  $\rho_{ma} = X/K$  in steady state.

For the stochastic process what we call here the steady-state (or equilibrium) density refers to the expected density of the quasi-stationary distribution calculated from simulations [27]. During simulations, if early extinction is avoided, the expected number of individuals eventually plateaus and then remains stable during the remainder of the simulated time. The steady-state density is taken from this plateau value. The first thing we note is that the mean-field approximation provides a poor representation of the stochastic equilibrium density (Figure 1C dotted line). Applying the same procedure to (14), and noting that when the system is at equilibrium  $Y_{ij1} = Y_{ij2}$  (or solving system (15) in steady state), we find the equilibrium density for the PA and 1<sup>st</sup> order SEDA models to be given by formula (2). In Figure 1C we see that (2) provides very good agreement with the steady-state densities from the stochastic process (for densities larger than 50%). Also, we again notice that the 2<sup>nd</sup> order improves slightly over the 1<sup>st</sup> order approximation (especially at lower densities).

Finally, we note that when the initial number of individuals,  $n_0$ , is small, extinction events can be caused by random fluctuations around small numbers. Indeed, the probability of early extinction is at least  $(D/(D + L))^{n_0}$ . However, unless  $n_0$  is quite small, there are parameter regions where early extinction is very unlikely. In particular, during simulations for Figure 1C extinction never occurred for all points that were tested with  $D/L < 0.62$  ( $n_0 = 13$ ). For  $D/L \geq 0.62$  on the other hand, population extinction always occurred, even when simulations started with a completely full grid. (For more on extinction from low numbers see [28, 29].)

## 4.2 Steady-state density for the Moore neighborhood

Moore neighborhoods can be defined in terms of the  $\ell_\infty$  distance, which states that  $\text{dist}(x_{ij}, x_{lk}) = \max(|i - l|, |j - k|)$ . The Moore neighborhood of radius one of a site  $a$ , can then be described as  $a$  and all sites that lie one unit of distance apart from  $a$  (8 neighbors in total). When dealing with Moore neighborhoods, in addition to the variables  $Y_{ij1} = \langle x_{ij}x_{i,j+1} \rangle$  and  $Y_{ij2} = \langle x_{ij}x_{i,j-1} \rangle$ , it is useful to introduce the quantities  $Y_{ij3} = \langle x_{ij}x_{i-1,j+1} \rangle$  and  $Y_{ij4} = \langle x_{ij}x_{i+1,j+1} \rangle$ . We can then use these variables to approximate the steady-state density of the system. Following the general methodology employed in the paper, we begin by writing ODEs for the rate of change of the variables  $U_{ij} = \langle x_{ij} \rangle$ ,  $Y_{ij1}$ ,  $Y_{ij2}$ ,  $Y_{ij3}$ , and  $Y_{ij4}$ . The resulting equations include objects of type  $P(b = 1, a = 0, c = 1)$ , where  $b$  and  $c$  are two distinct sites in the Moore neighborhood of radius one of a third site  $a$ . To proceed in the same way as for the von Neumann model, we apply the approximation in Eq. (12) to all triplets with  $\text{dist}(b, c) = 2$ . As a result, new variables must be added to the system. After symmetrizing for the steady-state analysis, we obtain a system of five equations (instead of the two for the von Neumann case (15)). We present and solve these equations numerically in Appendix E.

There is, however, a way to simplify the equations that allows for an analytical solution. Given a triplet,  $\{a, b, c\}$ , that satisfies the conditions previously described, we can apply approximation (12) *regardless* of the distance separating  $b$  and  $c$ . This approach leads directly to a closed system of ODEs. As before, to perform the steady-state analysis, we drop the coordinate subscripts for all

variables in the system, and find that the steady-state values for  $Y_1, Y_2, Y_3$  and  $Y_4$  are all the same. Simply calling this steady state  $Y$  leads to the equilibrium equations:<sup>1</sup>

$$\begin{aligned} 0 &= L(U - Y) - DU \\ 0 &= \frac{7}{4}L(U - Y)^2/(1 - U) + \frac{1}{4}L(U - Y) - 2DY \end{aligned} \quad (24)$$

Solving this last system for  $U$ , we find the closed-form approximation for the Moore neighborhood equilibrium density (4). This formula fits the numerically obtained data remarkably well (see Figure A7), and is only slightly less accurate than the more cumbersome method of decoupling used in Appendix E. This same simplifying approach can be used to find an approximation,  $\rho_H$ , for the steady-state density in a hexagonal (honeycomb) lattice, where each node has six nearest neighbors, see formula (3). The order relation between the approximate densities,  $\rho_{vN} \leq \rho_H \leq \rho_M$ , reflects what occurs in stochastic simulations, where the steady-state density increases with the number of neighbors.

Figure 7 plots the equilibrium density formulas for the mass-action, von Neumann, and Moore models. As we noted, spatial restrictions reduce the equilibrium density. In this sense, the von Neumann model imposes stronger spatial restrictions than the Moore model (4 vs. 8 nearest neighbors per site). The corresponding equilibrium density is therefore lower in the von Neumann model. It is important to note that formulas (2) and (4) capture this behavior, while the mean-field representations do not. Indeed, although the mass-action model and the spatial mean-field models for von Neumann (Eq. (7)) and Moore (not shown) have different propagation speeds, they all have the same steady-state density.

## 5 Population expansion rate

In this section we are interested in approximating the expected growth rate of a 2D population expanding radially from an origin  $o$  in an infinite grid. Under these conditions, when the population is large enough, the region of the grid colonized by the population up to a time  $t$  will roughly resemble a disk (see, for example, initial conditions in Figure 6). It is possible to derive approximate expressions for the expansion rate of these disks, as colonization proceeds.

Let  $A(t)$  be the area of the expanding region, and  $M(t)$  the total number of occupied sites. In the region's interior the density of occupied sites will be near equilibrium and thus we will have the relation:  $M(t) \approx A(t)\rho$ , where  $\rho$  is the steady-state density of occupied sites. We can then define the radius,  $R$ , and circumference,  $C$ , of the disk-like region in terms of  $M$ :

$$A = \pi R^2, \quad C = 2\pi R = 2\sqrt{\pi A} \approx 2\sqrt{\frac{\pi M}{\rho}}. \quad (25)$$

In the colonized region's interior, divisions exactly balance deaths; the number of individuals only increases through the dynamics on its boundary or surface, where there is no such balance. For this reason, we want to estimate the number of surface sites of a disk-like region. Let us begin by considering a circle of radius  $r$  and center  $o$  with coordinates  $(i_o, j_o)$  in a rectangular grid. We define the surface points of the circle as those with coordinates  $(i, j)$  such that (i)  $(i - i_o)^2 + (j - j_o)^2 \leq r^2$  and (ii) the point has at least one nearest neighbor,  $(i_1, j_1)$ , that lies outside of the circle, i.e.:  $(i_1 - i_o)^2 + (j_1 - j_o)^2 > r^2$ . Such points are denoted as blue dots in Figure 8A, which illustrates this for the von Neumann neighborhood. We find numerically that for large  $r$  the number of sites in the circle's surface  $\approx \beta \times 2\pi r$ , where  $\beta$  is constant that depends on the type of neighborhood

---

<sup>1</sup>Note that if we use this simplification for the von Neumann neighborhood, we recover 1st order SEDA.

used. Hence by analogy, we estimate that the number of surface sites,  $S(t)$ , of a stochastic disk-like region is:

$$S \approx \beta \times 2\pi R \approx \beta \times 2\sqrt{\frac{\pi M}{\rho}} \quad (26)$$

We are only interested in the dynamics at the surface, where the approximate number of individuals is  $S\rho$ . The net growth rate of the system is  $L - D$ ; however, at the surface only the fraction of the growth rate directed towards the outside of the disk,  $\nu$ , counts towards expansion. The other fraction of the surface growth,  $1 - \nu$ , is directed towards the interior of the disk-like region, where we assume that births and deaths are balanced. This fraction,  $\nu$ , is equal to the average number of exterior and surface neighbors that an individual at the surface has, divided by four. The approximate total growth rate is then equal to  $\nu(L - D)\rho S$ , where the inclusion of  $\sqrt{\rho}$  introduces a non-linear term. The equation for the total population can be written as:

$$\frac{dM}{dt} = \nu\rho S(L - D) = \nu\beta \times 2\sqrt{\pi\rho M}(L - D) = a\sqrt{M}, \quad (27)$$

where the expansion rate  $a$  is given by

$$a = 2\nu\beta\sqrt{\pi\rho} (L - D), \quad (28)$$

and quantities  $\nu$ ,  $\rho$ , and  $\beta$  depend on the type of neighborhood used. The expansion rate in (28) was derived from first principles, where all components have a physical meaning. It is worth mentioning however, that a simple linear regression of the data in Figure 8 would result in a tighter fit for  $a$ .

### 5.1 Expansion rate for the von Neumann neighborhood

Using the von Neumann model, we can numerically estimate the number of surface points in a circle of a given radius, which leads to the value  $\beta_{vN} \approx 0.9$ , see Figure 8A. The density formula is given by equation (2).

The next step in our derivation is to find an estimate for  $\nu_{vN}$ . Let us begin again by considering a circle. For each point in a circle's surface, we want to determine how many of its four nearest neighbors lie outside the circle, belong to its surface, or to the circle's interior. In Figure 8A a circle's surface points are marked as blue dots; and for illustrations purposes, the neighbors of four of these points (A, B, C, and D) are enclosed in red diamonds. For point A, two of its neighbors belong to the surface and one neighbor lies outside the circle. For point B, two neighbors are in the interior, and two lie outside the circle. For point C, one neighbor is in the surface and two lie outside the circle. For point D, one neighbor is in the surface and one lies outside. Hence, for points A and C, three out of their four neighbors are not in the interior. For points B and D, two of their neighbors are not in the interior. Increasing the circle's radius and calculating the average fraction of neighbors that lie either outside the circle or in its surface, we find numerically that this quantity,  $\nu_{vN} \approx 0.65$ . Figure 8B plots the values of the growth rate parameter  $a$  obtained from stochastic simulations (blue dots) compared with formula (28) (blue solid line).

### 5.2 Expansion rate for the Moore neighborhood

Using the method of Figure 8A adapted to the Moore neighborhood, we find numerically that  $\beta_M \approx 1.27$ . The density formula is given by the solution of system (A8-A12), or more concisely (with slightly larger error), by Eq. (4). Similarly, the average fraction of neighbors that are not in the circle's interior is given by  $\nu_M \approx 0.70$ . Figure 8B compares the results from stochastic simulations with formula (28), using  $\beta_M$  and  $\nu_M$  for  $\beta$  and  $\nu$ .

In Figure 8B we also see that expansion happens faster under the Moore neighborhood. This can be intuitively understood by noting that with a larger number of points that count as neighbors, an individual has more choices for placing its offspring. In the case of a mass action (not shown) expansion is fastest and exponential in time.

## 6 Discussion

In this paper we developed deterministic approximations for the expected trajectories of a two-dimensional stochastic birth-death process. In particular, we focused on modeling 2D growth expanding radially from an origin  $o$ , a problem known in the literature as range expansion. We began by considering approximations based on the decoupling ideas of the *pair approximation* (PA); we referred to these approximations as *spatially explicit decoupling approximations*, or SEDA. For each SEDA we defined an order: A SEDA of  $n^{\text{th}}$  order preserves correlations between neighbors that are  $n$  or less units of distance apart from each other. We found that  $1^{\text{st}}$  order SEDA approximates the results from the stochastic process better than the mean-field or PA models; and  $2^{\text{nd}}$  order improves on the  $1^{\text{st}}$  order approximation. However, none of these models exhibit good time series agreement with the stochastic process.

There are two important differences between PA and SEDA. 1) PA models are non-spatial. They track only the total number of individuals, but not the spatial location of each individual. SEDA is fully spatial. 2) PA models only consider correlations of pairs, while depending on the order, SEDA models can preserve correlations for larger groups of neighbors (e.g., up to quintuplets in  $2^{\text{nd}}$  order equations).

Next, we developed what we called *radial decoupling approximations*, or RDA. Here, an approximation involving a triad of sites depends on the location of the triad’s center relative to the population origin. A system based only on RDA does not have a unique steady state; RDA however, will be very useful when combined with SEDA. This approach lead us to the *trigonometric decoupling approximations*, or TDA. The name comes from the use of trigonometric functions in the approximations. We find that the TDA provides very good agreement with the stochastic process. We then revisited  $1^{\text{st}}$  order SEDA, and found that scaling time by a suitable parameter also produces very good agreement with stochastic results.

The methods described above allow us to approximate the steady-state density of populations (or the density in the core of expanding colonies). In particular, we provide three simple formulas that approximate the equilibrium density: for the von Neumann and Moore neighborhoods on a square lattice, and for a honeycomb neighborhood on a hexagonal lattice, see Eqs. (2, 3, 4). For the same death-to-birth ratio, the grid is more packed under the Moore neighborhood, because of the availability of more neighbors per site. As a consequence, the equilibrium density corresponding to the Moore neighborhood is higher and closer to that of mass action. A general formula that provides an approximation for the steady-state density as a function of the number of neighbors is given by equation (5). It describes the three cases in 2D that were mentioned above, and can also be derived in 3D for the von Neumann and Moore neighborhoods. The validity of this formula for other cases remains to be checked.

Finally, we turned our attention to the expected growth rate of an expanding population in an infinite grid. By focusing on the dynamics at the population’s surface (or boundary), we found a simple explicit formula, Eq. (27), that estimates the evolution of the total number of individuals as a function of time. The growth law in (27) is the so called “surface growth” law [30], previously described in modeling literature [31–35]. Equation (28) provides a method to approximate the rate of surface growth from the “microscopic” rules and rates that govern the spatial birth-death

process. This method involves knowledge of a population steady-state density, and the geometric properties of disk-like objects on a square lattice, both of which depend on neighborhood type.

The methodology developed in the article can be adapted to include three-dimensional growth and other grid metrics. In 3D there are four equations per site for all 1<sup>st</sup> order approximations using the  $\ell_1$  metric. SEDA and TDA approximations can also be developed for Moore neighborhoods (based on the  $\ell_\infty$  norm). Using Moore neighborhoods in 2D, for example, leads to 10 equations per grid point for 1<sup>st</sup> order SEDA. Another important extension of the methodology is the inclusion of populations with more than one species. For example, in 2D with the  $\ell_1$  metric, for a two species birth-death process there are ten equations per point for 1<sup>st</sup> order approximations: two for the expected value of singletons (one per species), four for correlations of pairs of the same species, and four more for correlations of mixed pairs. For more complex models, such as those involving two or more species, the process of generating equations can be automated using *Mathematica*, by first working out a pattern and then implementing equation generation in a program, a methodology similar to that used in [36].

Applying the methodology to more than one species can lead to important biological applications. For example, in the context of tumor growth, a two species birth-death model can be easily adapted to account for feedback interactions between tumor stem cells and differentiated cells [37]. Similar adaptations can be used to model viral infection and the interplay between infected and uninfected cells [38]. Another fundamental application is studying mutant dynamics in a spatial setting, which is relevant to a host of phenomena: ranging from 2D bacterial evolution in biofilms, to 3D evolutionary dynamics of cancer. In particular, the ideas used to estimate the population's expected growth rate (for one specie), could be applied to approximate the expected number of mutants as a function of time. The extensions to the theory and approximations discussed here can form the basis of these and other applications, and will be the focus of future work.

## Author contributions

Designed research: IARB, DW, NLK. Performed research: IARB, NLK. Wrote the paper: IARB, NLK.

## References

- [1] Qi Wang and Tianyu Zhang. Review of mathematical models for biofilms. *Solid State Communications*, 150(21-22):1009–1022, 2010.
- [2] Katarzyna A Rejniak and Alexander RA Anderson. Hybrid models of tumor growth. *Wiley Interdisciplinary Reviews: Systems Biology and Medicine*, 3(1):115–125, 2011.
- [3] J Landry, JP Freyer, and RM Sutherland. A model for the growth of multicellular spheroids. *Cell Proliferation*, 15(6):585–594, 1982.
- [4] JE Barralet, L Wang, M Lawson, JT Triffitt, PR Cooper, and RM Shelton. Comparison of bone marrow cell growth on 2d and 3d alginate hydrogels. *Journal of materials science: materials in medicine*, 16(6):515–519, 2005.
- [5] Arthur L Koch. The growth of viral plaques during the enlargement phase. *Journal of theoretical biology*, 6(3):413–431, 1964.
- [6] Joaquim Fort and Vicenç Méndez. Time-delayed spread of viruses in growing plaques. *Physical review letters*, 89(17):178101, 2002.
- [7] Stephen T Abedon and John Yin. Bacteriophage plaques: theory and analysis. In *Bacteriophages*, pages 161–174. Springer, 2009.

- [8] Sergei Fedotov, David Moss, and Daniel Campos. Stochastic model for population migration and the growth of human settlements during the neolithic transition. *Physical Review E*, 78(2):026107, 2008.
- [9] Hannes Taubenböck, Michael Wurm, Christian Geiß, Stefan Dech, and Stefan Siedentop. Urbanization between compactness and dispersion: designing a spatial model for measuring 2d binary settlement landscape configurations. *International Journal of Digital Earth*, pages 1–20, 2018.
- [10] Joana Moreira and Andreas Deutsch. Cellular automaton models of tumor development: a critical review. *Advances in Complex Systems*, 5(02n03):247–267, 2002.
- [11] Inés Santé, Andrés M García, David Miranda, and Rafael Crecente. Cellular automata models for the simulation of real-world urban processes: A review and analysis. *Landscape and Urban Planning*, 96(2):108–122, 2010.
- [12] Gary An, Qi Mi, Joyeeta Dutta-Moscato, and Yoram Vodovotz. Agent-based models in translational systems biology. *Wiley Interdisciplinary Reviews: Systems Biology and Medicine*, 1(2):159–171, 2009.
- [13] Helen Byrne and Dirk Drasdo. Individual-based and continuum models of growing cell populations: a comparison. *Journal of mathematical biology*, 58(4):657–687, 2009.
- [14] Zhihui Wang, Joseph D Butner, Romica Kerketta, Vittorio Cristini, and Thomas S Deisboeck. Simulating cancer growth with multiscale agent-based modeling. In *Seminars in cancer biology*, volume 30, pages 70–78. Elsevier, 2015.
- [15] Nicolaas Godfried Van Kampen. *Stochastic processes in physics and chemistry*, volume 1, pages 96 – 129. Elsevier, third edition, 2007.
- [16] V Volpert and S Petrovskii. Reaction–diffusion waves in biology. *Physics of life reviews*, 6(4):267–310, 2009.
- [17] Stephen P Ellner, Akira Sasaki, Yoshihiro Haraguchi, and Hirotsugu Matsuda. Speed of invasion in lattice population models: pair-edge approximation. *Journal of Mathematical Biology*, 36(5):469–484, 1998.
- [18] Stephen P Ellner. Pair approximation for lattice models with multiple interaction scales. *Journal of theoretical biology*, 210(4):435–447, 2001.
- [19] Jaewook Joo and Joel L Lebowitz. Pair approximation of the stochastic susceptible-infected-recovered-susceptible epidemic model on the hypercubic lattice. *Physical Review E*, 70(3):036114, 2004.
- [20] Chris T Bauch. The spread of infectious diseases in spatially structured populations: an invasy pair approximation. *Mathematical biosciences*, 198(2):217–237, 2005.
- [21] Jerome Benoit, Ana Nunes, and M Telo da Gama. Pair approximation models for disease spread. *The European Physical Journal B-Condensed Matter and Complex Systems*, 50(1-2):177–181, 2006.
- [22] Emanuele Pugliese and Claudio Castellano. Heterogeneous pair approximation for voter models on networks. *EPL (Europhysics Letters)*, 88(5):58004, 2009.
- [23] Xiao-Feng Luo, Xiaoguang Zhang, Gui-Quan Sun, and Zhen Jin. Epidemical dynamics of SIS pair approximation models on regular and random networks. *Physica A: Statistical Mechanics and its Applications*, 410:144–153, 2014.
- [24] Angélica S Mata, Ronan S Ferreira, and Silvio C Ferreira. Heterogeneous pair-approximation for the contact process on complex networks. *New Journal of Physics*, 16(5):053006, 2014.
- [25] Hirotsugu Matsuda, Naofumi Ogita, Akira Sasaki, and Kazunori Satō. Statistical mechanics of population: the lattice Lotka-Volterra model. *Progress of theoretical Physics*, 88(6):1035–1049, 1992.
- [26] Michael A Gibson and Jehoshua Bruck. Efficient exact stochastic simulation of chemical systems with many species and many channels. *The journal of physical chemistry A*, 104(9):1876–1889, 2000.
- [27] Erik A van Doorn and Philip K Pollett. Quasi-stationary distributions for discrete-state models. *European journal of operational research*, 230(1):1–14, 2013.



- [28] Ignacio A Rodriguez-Brenes, Dominik Wodarz, and Natalia L Komarova. Quantifying replicative senescence as a tumor suppressor pathway and a target for cancer therapy. *Scientific reports*, 5:17660, 2015.
- [29] Andrew Hofacre, Dominik Wodarz, Natalia L Komarova, and Hung Fan. Early infection and spread of a conditionally replicating adenovirus under conditions of plaque formation. *Virology*, 423(1):89–96, Feb 2012.
- [30] M Block, E Schöll, and D Drasdo. Classifying the expansion kinetics and critical surface dynamics of growing cell populations. *Physical review letters*, 99(24):248101, 2007.
- [31] Antonio Brú, Sonia Albertos, José Luis Subiza, José López García-Asenjo, and Isabel Brú. The universal dynamics of tumor growth. *Biophysical journal*, 85(5):2948–2961, 2003.
- [32] Natalia L Komarova and Dominik Wodarz. Ode models for oncolytic virus dynamics. *Journal of theoretical biology*, 263(4):530–543, 2010.
- [33] Ignacio A Rodriguez-Brenes, Natalia L Komarova, and Dominik Wodarz. Tumor growth dynamics: insights into evolutionary processes. *Trends in ecology & evolution*, 28(10):597–604, 2013.
- [34] Anne Talkington and Rick Durrett. Estimating tumor growth rates in vivo. *Bulletin of mathematical biology*, 77(10):1934–1954, 2015.
- [35] Hope Murphy, Hana Jaafari, and Hana M Dobrovolny. Differences in predictions of ode models of tumor growth: a cautionary example. *BMC cancer*, 16(1):163, 2016.
- [36] A Mahdipour-Shirayeh, A H Darooneh, A D Long, N L Komarova, and M Kohandel. Genotype by random environmental interactions gives an advantage to non-favored minor alleles. *Sci Rep*, 7(1):5193, 07 2017.
- [37] Ignacio A Rodriguez-Brenes, Natalia L Komarova, and Dominik Wodarz. Evolutionary dynamics of feedback escape and the development of stem-cell-driven cancers. *Proc Natl Acad Sci U S A*, 108(47):18983–8, Nov 2011.
- [38] Ignacio A Rodriguez-Brenes, Andrew Hofacre, Hung Fan, and Dominik Wodarz. Complex dynamics of virus spread from low infection multiplicities: Implications for the spread of oncolytic viruses. *PLoS computational biology*, 13(1):e1005241, 2017.

## Figure Legends

**Figure 1:** A) Spatial configuration of the expected population density at  $t = 19.5$ , for the stochastic (top) and  $1^{st}$  order SEDA model (bottom). Color bar indicates density. B) Expected total number of individuals as a function of time. Results from stochastic simulations (thick solid line) compared with the output of the mean-field model,  $1^{st}$  and  $2^{nd}$  order SEDA, and pair approximation (PA, thin solid line). In panels A) and B), death rate  $D = 1$ ; reproduction rate  $L = 4$ ; grid size  $129 \times 129$ . Initial conditions: 5 individuals at grid’s center. C) Steady-state density of occupied sites as a function of the death-to-birth ratio  $D/L$ . Stochastic results based on  $10^4$  or more independent simulations per point/curve. Initial conditions: 13 individuals at grid’s center. Confidence interval error bars are smaller than thickness of symbols/curves (not shown).

**Figure 2:** Panels show all geometric configurations for sites  $a, b$ , and  $c$  that satisfy  $\text{dist}(a, b) = \text{dist}(a, c) = 1$ , and  $\text{dist}(b, c) = 2$ . Clock-wise from top-right the configurations describe the sites in the probabilities  $P_{ijk}$  from  $k = 1, \dots, 6$  (Eq. (10)). The angles and semi-planes ( $\theta_{abc}$ ,  $H_b$  and  $H_c$ ) are used to determined which RDA approximation to use ( $\eta(\langle b \rangle - \langle ab \rangle)$  or  $\eta(\langle c \rangle - \langle ac \rangle)$ ), based on the location of  $a$  relative to the population origin  $o$ . See text for discussion and Table 1.

**Figure 3:** Weight coefficients for the trigonometric approximation. A) Best fit coefficients  $\hat{\alpha}_{ij1}$  vs. the angles  $\theta_{ij}$  for each site in the grid (scattered plot); trigonometric approximation (solid line). B)  $\alpha_1(\theta)$  is the average of all  $\hat{\alpha}_{ij1}$ , for which  $\theta_{ij} = \theta$  (dotted line). C)  $\alpha_4(\theta)$  and  $\alpha_6(\theta)$  (dotted and thin lines); trigonometric approximation (thick line).  $D = 0.1$ ;  $L = 4$ ; grid size  $45 \times 45$ . For the behavior of the other weight coefficients ( $\alpha_{ij2}, \alpha_{ij3}, \alpha_{ij5}$ ) see Table 1.

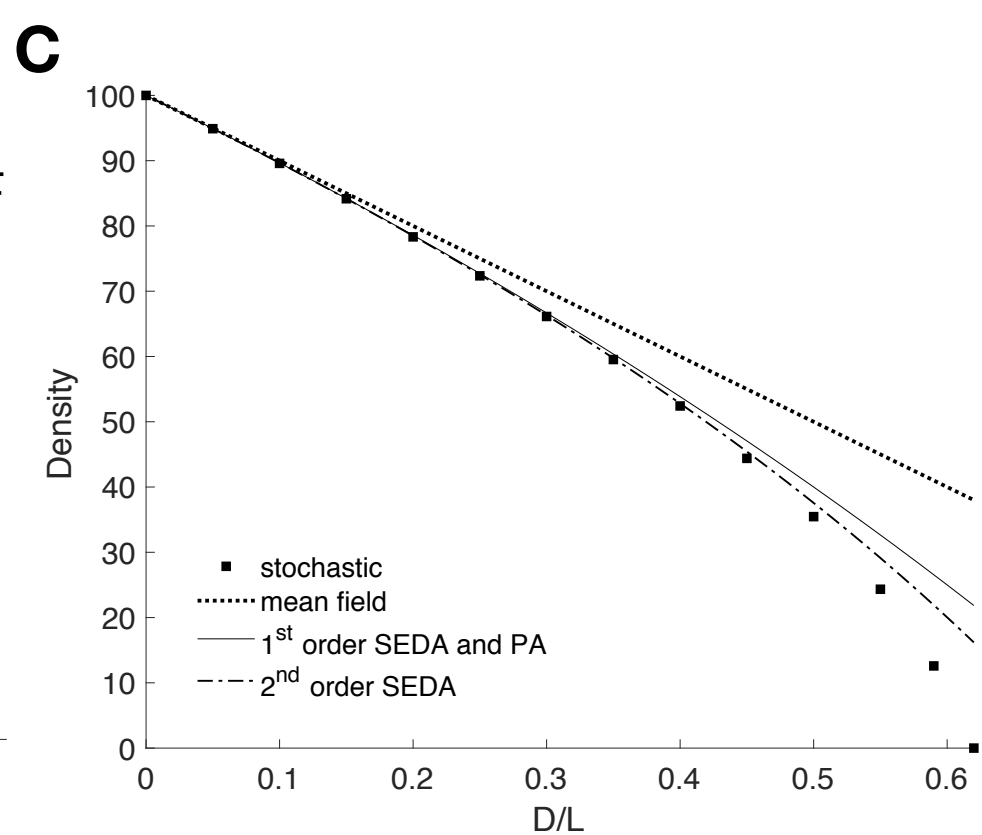
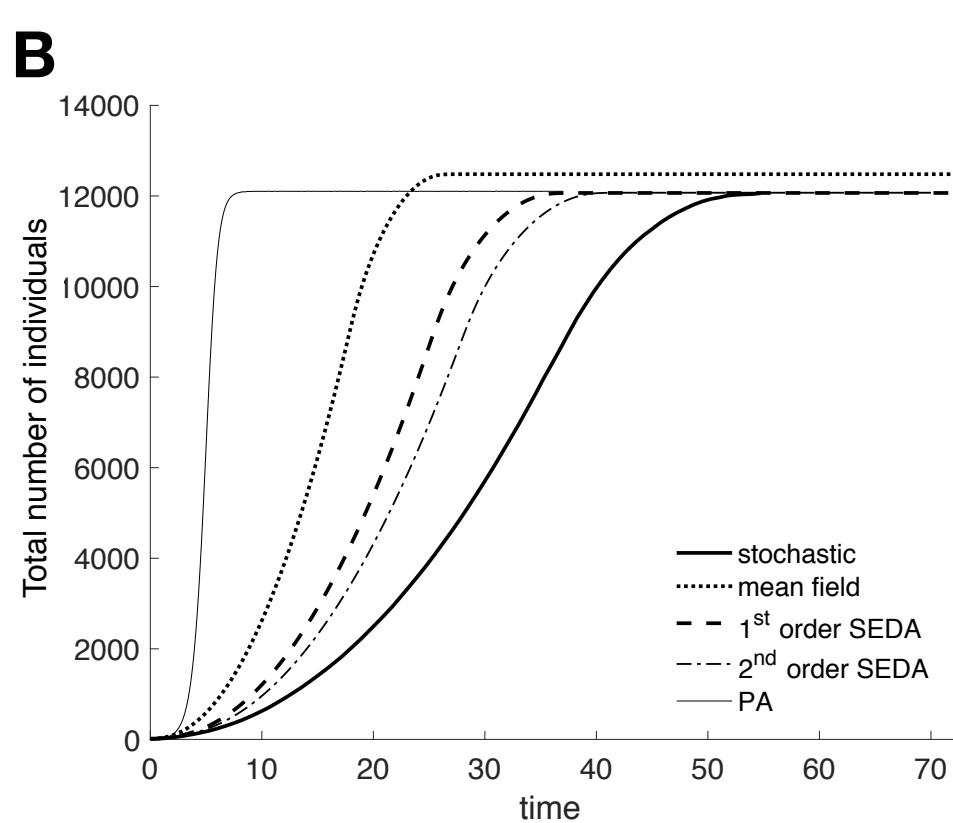
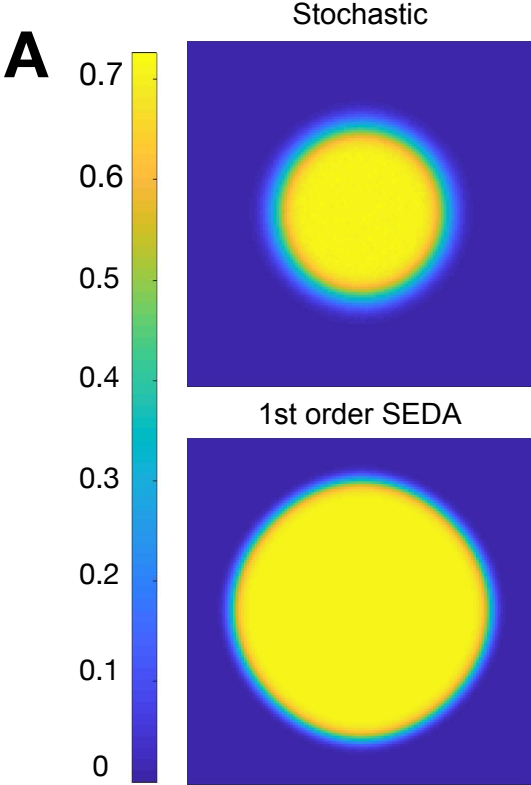
**Figure 4:** Expected total number of individuals as a function of time. Stochastic simulation results (blue) compared with the output of three deterministic models: mean field (red), SEDA (yellow), and TDA (purple). For all plots the reproduction rate  $L = 4$ . The death rates are: (A)  $D = 0.1$ ; (B)  $D = 1$ ; and (C)  $D = 1.5$ . Grid sizes indicated in bottom-right corner of each panel ( $N = 45^2$  or  $N = 129^2$ ). Stochastic results based on at least  $10^4$  independent simulations per curve (error bars smaller than thickness of curves, not shown).

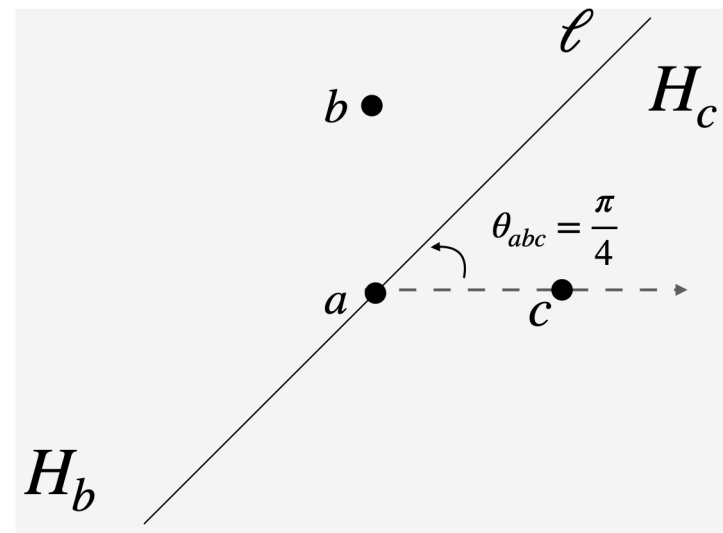
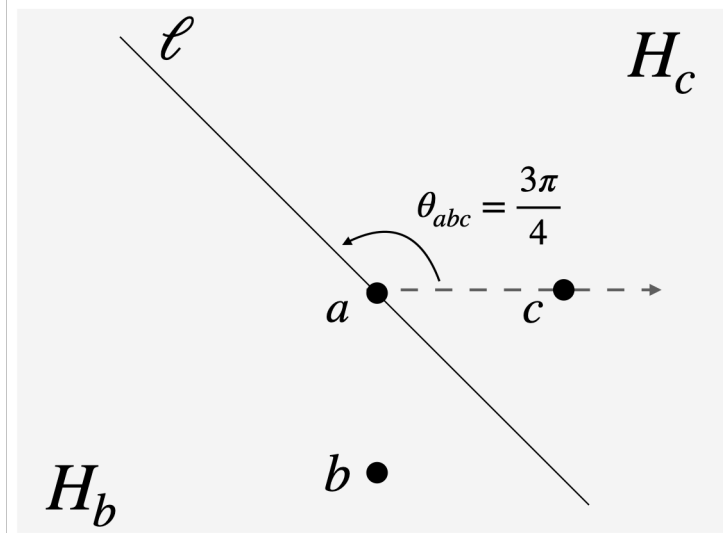
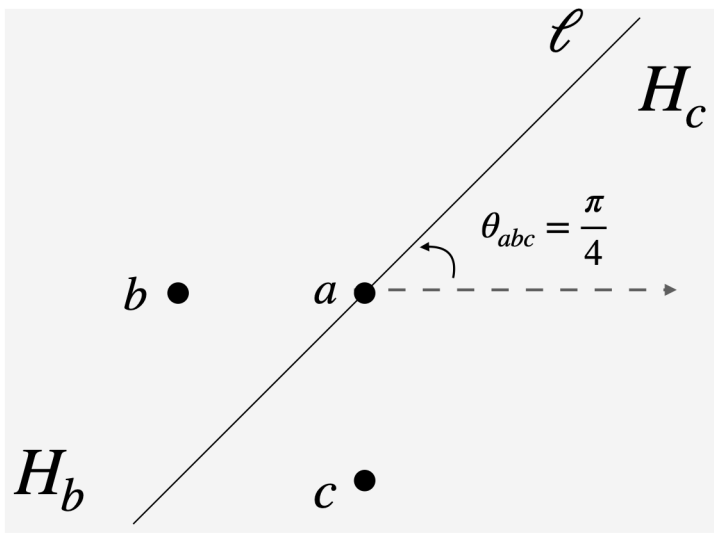
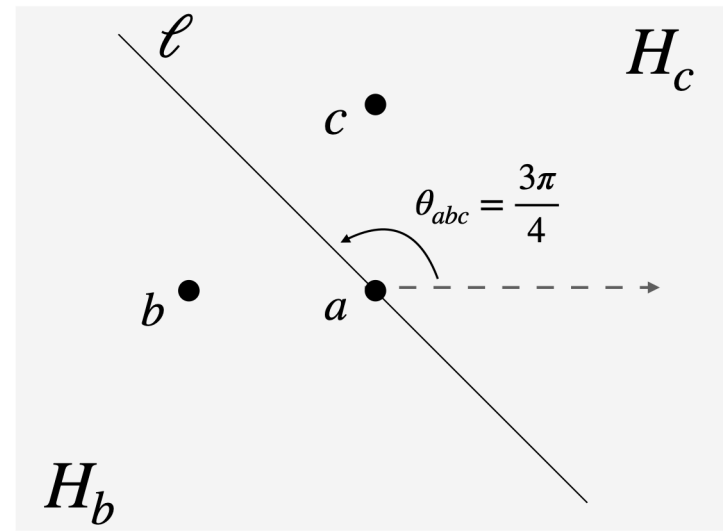
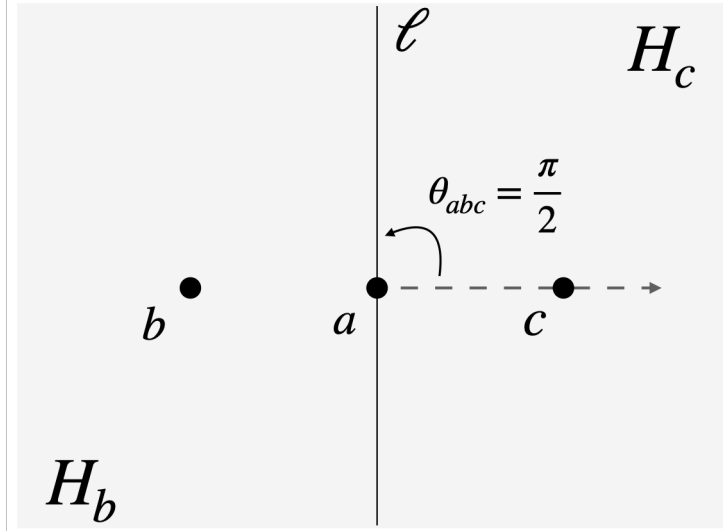
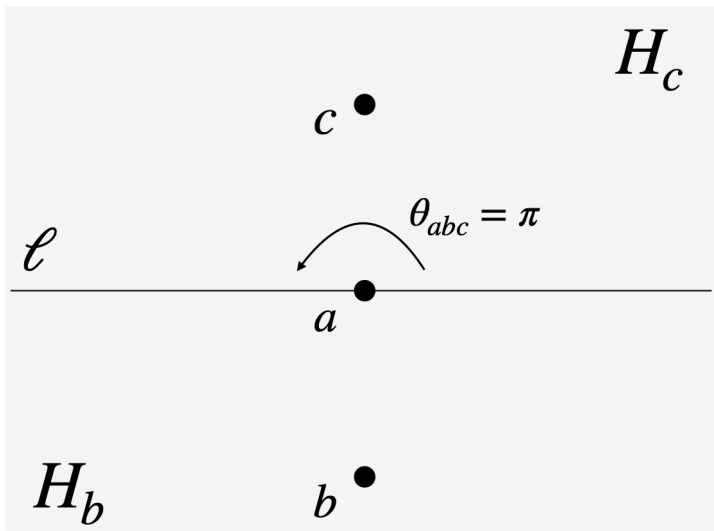
**Figure 5:** Time-scaled SEDA. A) Solid lines show the trajectories of the expected number of individuals as a function of time calculated from 5000 independent simulations per curve (error bars too small to plot). Dashed lines show time-scaled SEDA. B) Inverse of time scaling parameter,  $\alpha_{D/L}^{-1}$ , as a function of  $D/L$ . Curve plots the polynomial regression in Eq. 23 (adjusted coefficient of determination  $\bar{R}^2 > 0.99$ ). In all simulations  $L = 4$  and grid size is  $45 \times 45$ .

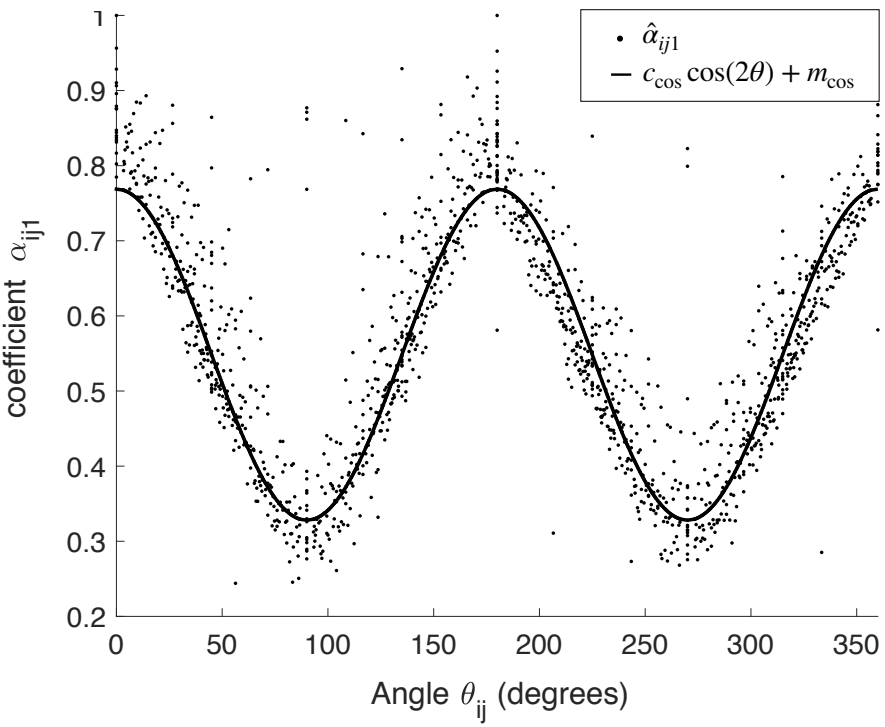
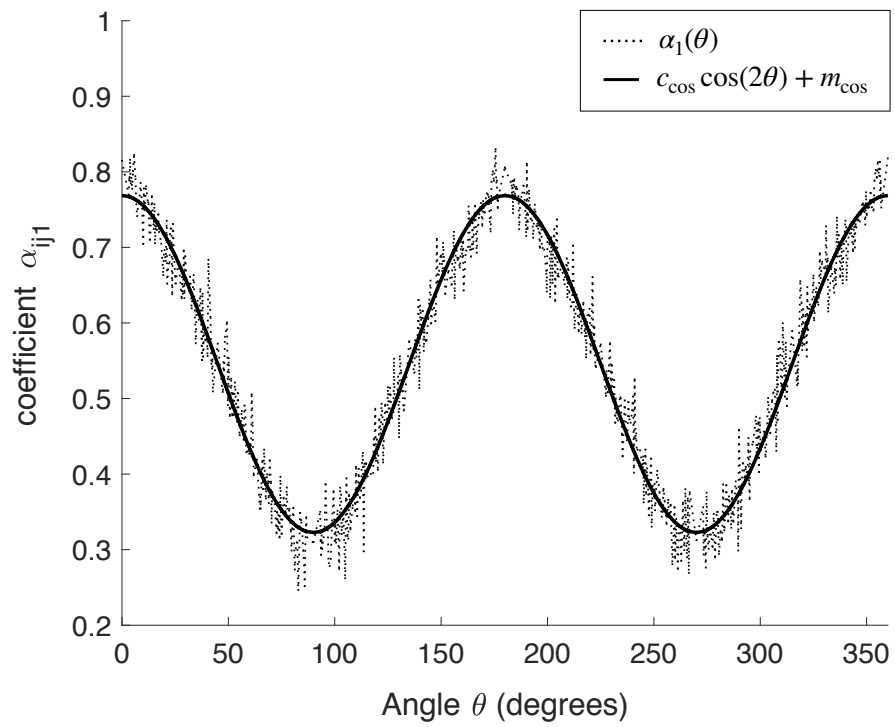
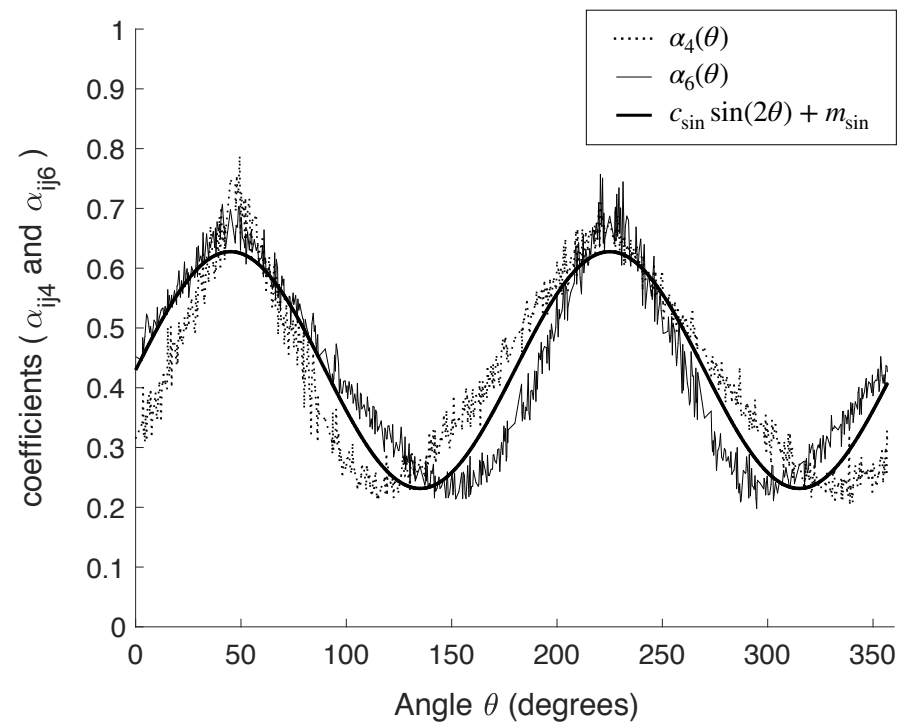
**Figure 6:** Expected number of individuals as a function of time in large grids. The initial conditions (random plaques) are shown on the left side of each panel (occupied sites are depicted in white, empty sites in black). A) Death rate  $D = 0.1$ , grid size  $1000 \times 1000$ , 18000 occupied sites at  $t = 0$  (1.8% of grid size). B) Death rate  $D = 1$ , grid size  $3163 \times 3163$ , 25000 occupied sites at  $t = 0$  (0.25% of grid size). In both panels the reproduction rate  $L = 4$ .

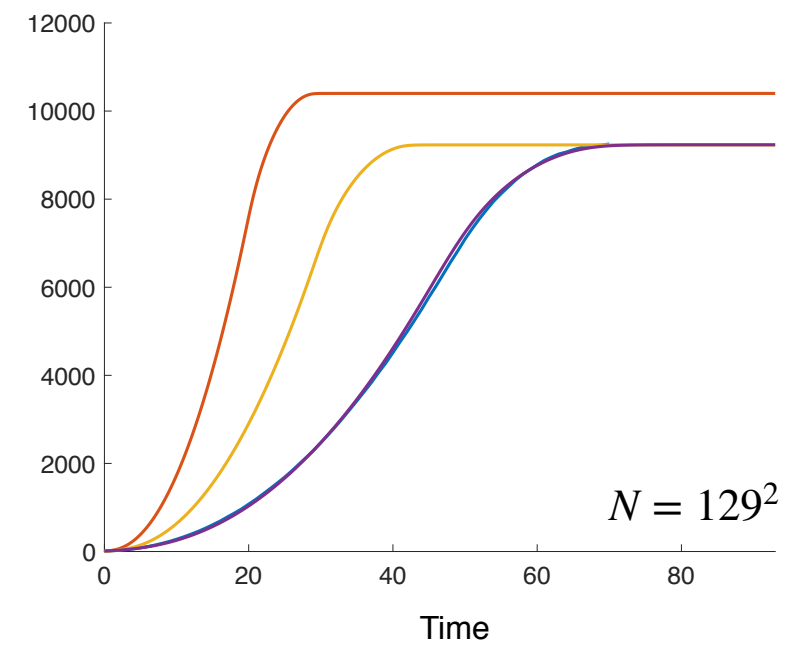
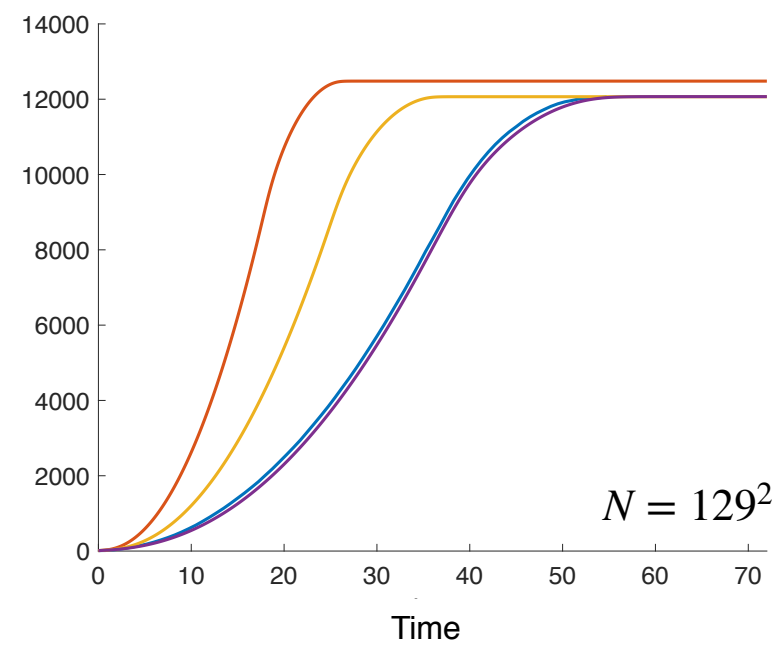
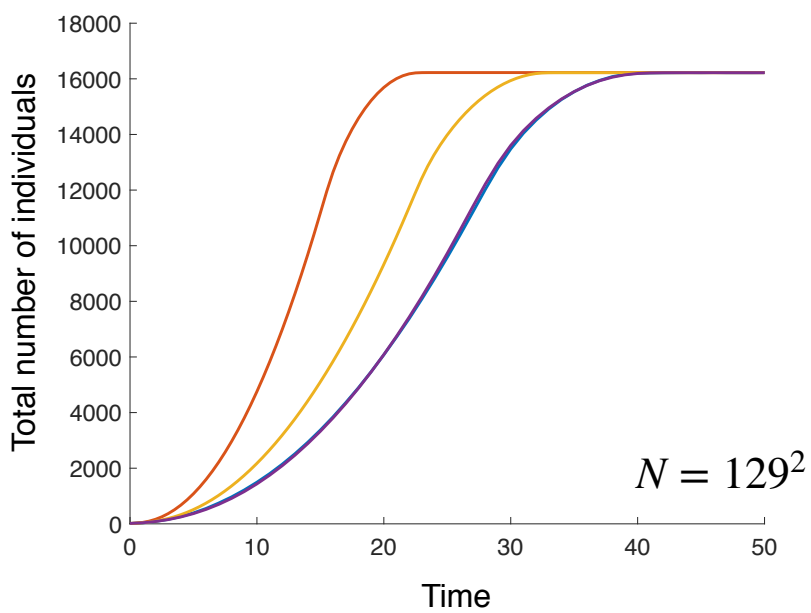
**Figure 7:** The equilibrium density in mass-action (mean-field), von Neumann, and Moore models, as functions of the death-to-divisions ration. The lines correspond to formulas (1, 2, 4).

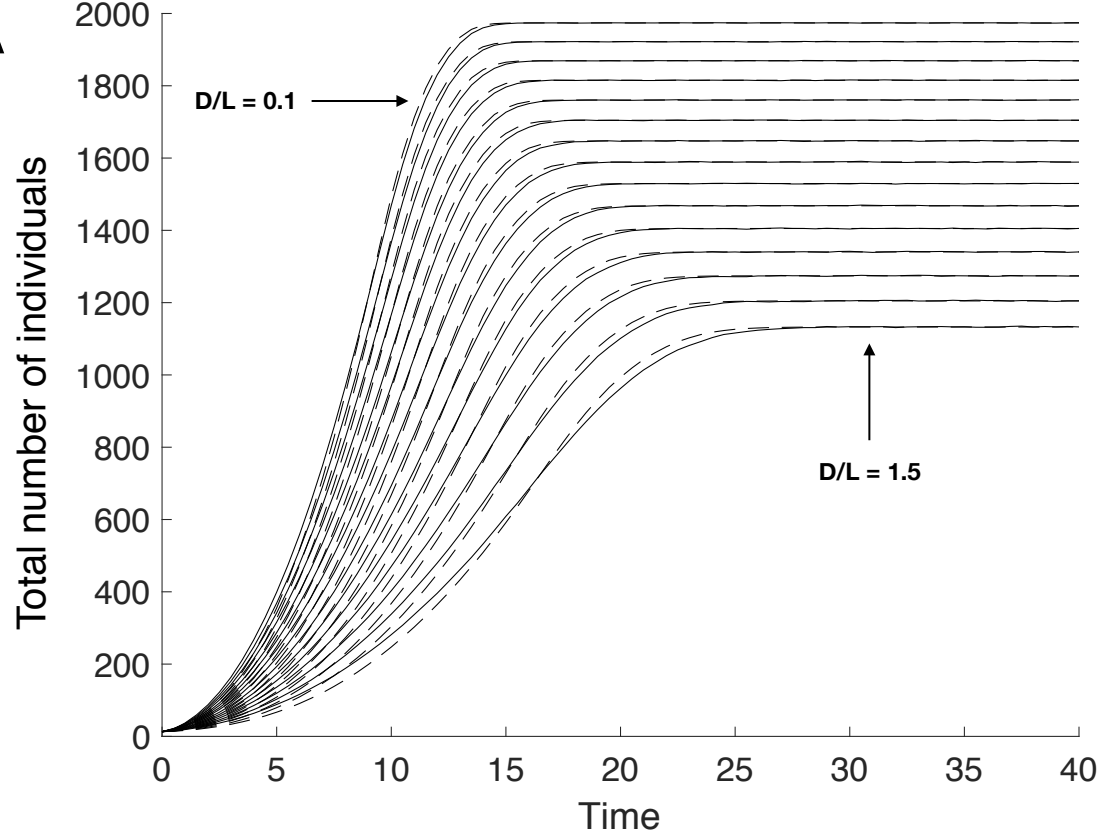
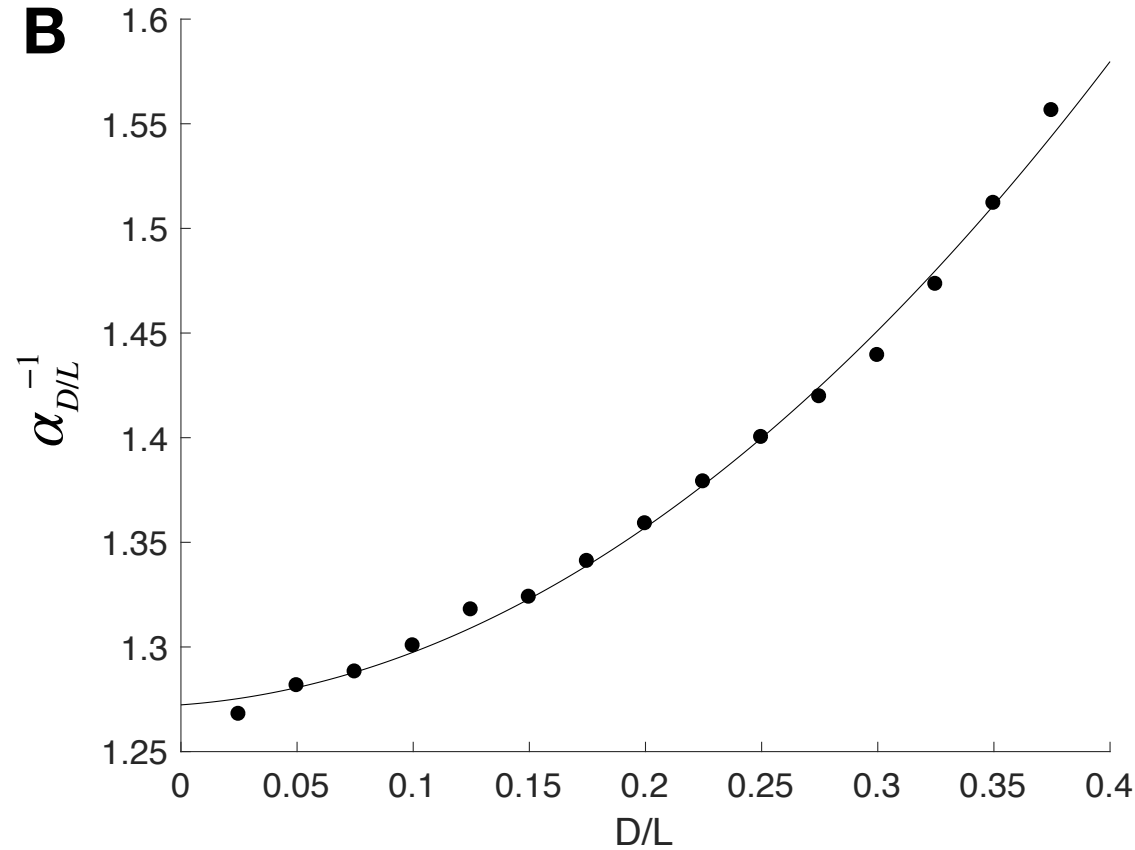
**Figure 8:** A) Surface points of a circular domain on a square grid. Calculations are demonstrated for the von Neumann model. For point A, two of its neighbors belong to the surface and one neighbor lies outside the circle. For point B, two neighbors are in the interim, and two lie outside the circle. For point C, one of the neighbors is part of the surface set and two lie outside the circle. For point D, one neighbor is part of the surface set and one lies outside the surface. B) Growth rate parameter  $a$  as a function of  $D/L$  (Eq. 27) for  $L = 4$ , for von Neumann and Moore neighborhood models. Calculated from stochastic simulations (dots) and formulas (solid lines).

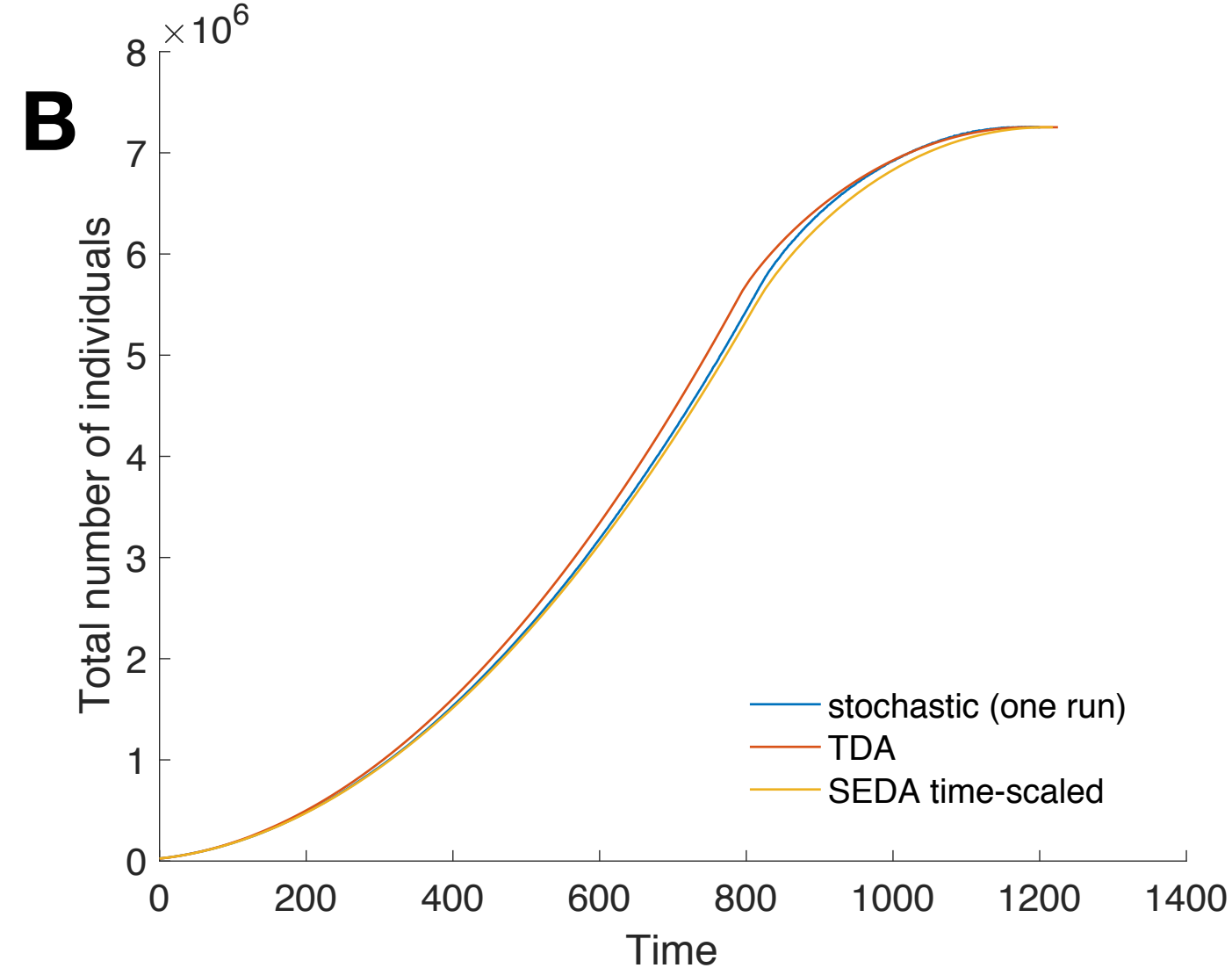
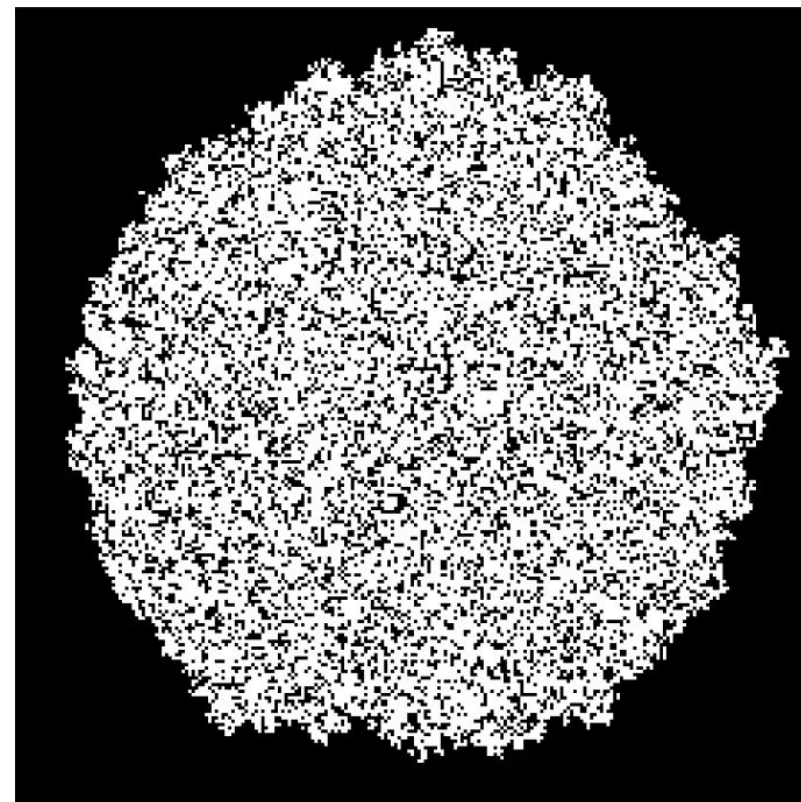
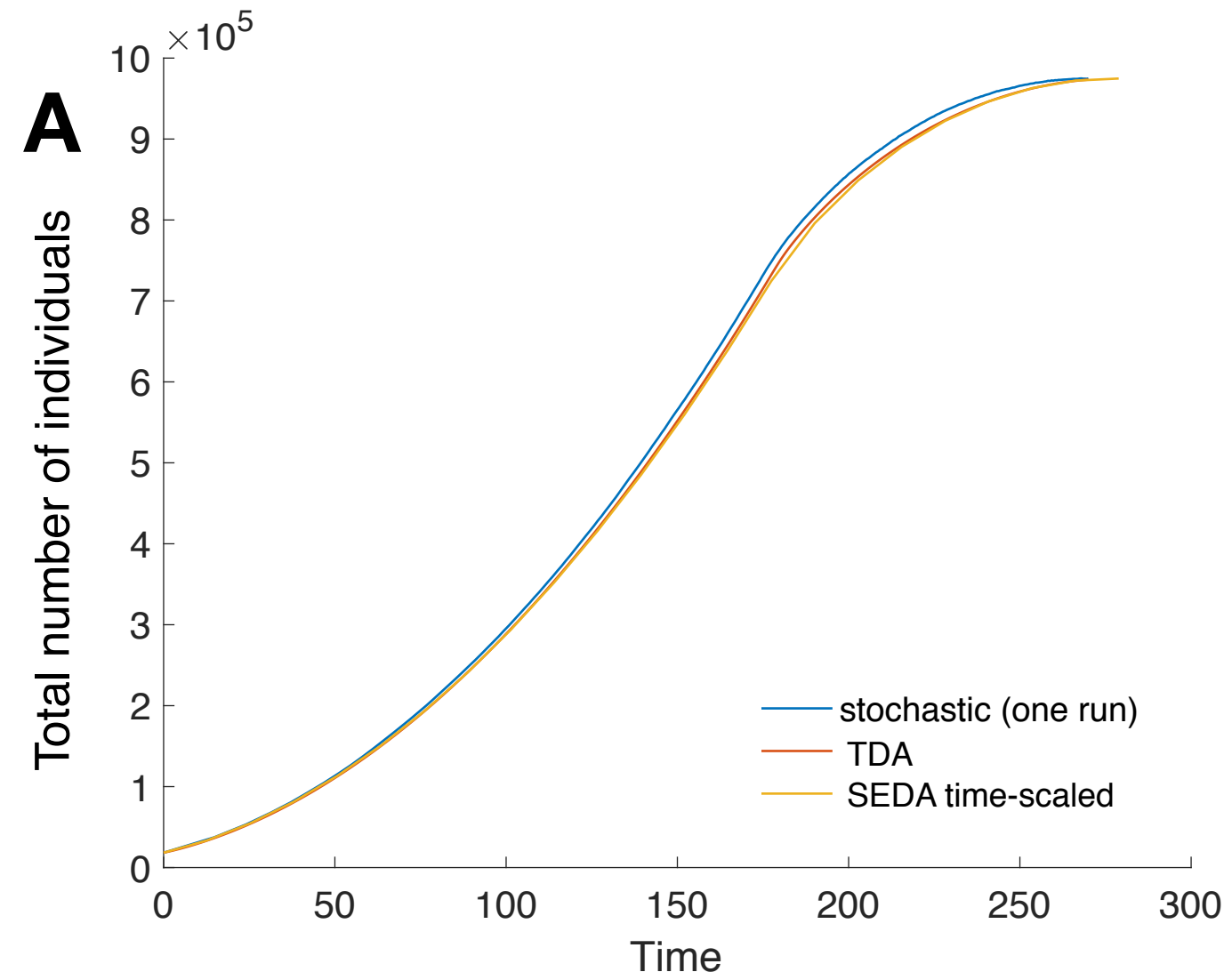
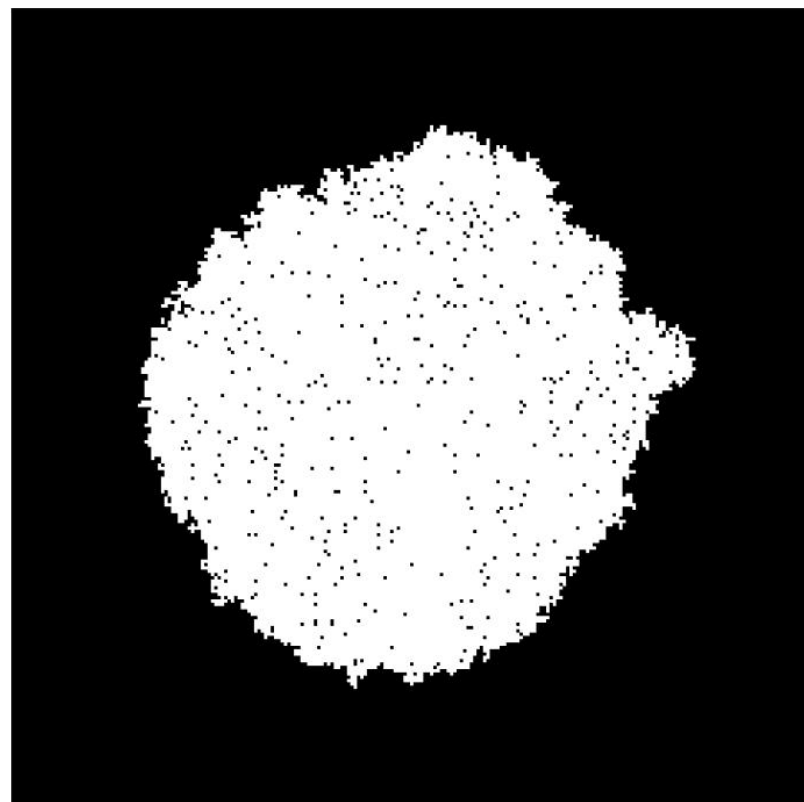




**A****B****C**



**A****B**





Equilibrium density

Mass-action

Moore

Von Neumann

1.0  
0.9  
0.8  
0.7  
0.6  
0.5  
0.4

0.0

0.1

0.2

0.3

0.4

0.5

$D/L$

